Electronic Supplementary Information (ESI)

Ternary hybrids as efficient bifunctional electrocatalysts derived from bimetallic metal-organic-frameworks for overall water splitting

Xiao Li, Xinlong Wang, Jie Zhou, Lu Han, Chunyi Sun, Qingqing Wang and Zhongmin Su**

National & Local United Engineering Laboratory for Power Battery, Institute of Functional Materials Chemistry, Northeast Normal University, Changchun, Jilin, 130024, China.

*E-mail: zmsu@nenu.edu.cn,

Table of Contents

1. Experimental Section

Materials and method

Commercial chemicals used in reactions were purchased without purification. IR spectrum was conducted using KBr pellets with an Alpha Centaurt FT/IR spectrophotometer ranging from 4000 to 400 cm^{-1}. Elemental analyses are performed with a Perkin-Elmer 240C elemental analyzer. TGA was performed under nitrogen atmosphere with a ramping rate of 10 °C min-1 utilizing a Perkin-Elmer TG-7 analyzer from 25 °C to 800 °C. PXRD patterns were gathered by a Siemens D5005 diffractometer with Cu-Kα (λ = 1.5418Å) radiation ranging from 3° to 80° at 293K with a rate of 5 min-1. A JY Labram HR 800 is carried out for the Raman spectra. A SU8000 ESEM FEG microscope was utilized to obtain the interrelated energy dispersive X-ray detector (EDX) spectra.The N_2 sorption tests were measured on automatic volumetric adsorption equipment (Belsorp mini II). The TEM was accomplished on a JEOL-2100F transmission electron microscope. The gas product in electrocatalytic reaction was measured by Shimadzu Gas Chromatography.

Synthesis of CoMo-MOF and NiMo-MOF

[CoMo(bimbp)$_2$O$_4$] A mixture containing $Co(NO_3)_2 \cdot 6H_2O$ (30 mg), $(NH_4)_6Mo_7O_{24} \cdot 4H_2O$ (24 mg) and bimbp (bimbp = 4,4'-bis(imidazolyl)bipheny, 30 mg) was firstly dissolved in 8 mL water. Then, we use a solution of 2 mol L^{-1} NaOH to adjust the mixture until the pH value reached about 6.0. Finally, the mixture was placed in to a 23 mL Teflon reactor after stirring at room temperature for 30min and further sealed, heating at 100 °C for 72h. After naturally cooled down, red block of crystals were filtered. Yield: 42 mg (57% yield based on bimbp). Anal. calcd for $C_{36}H_{28}CoMoN_8O_4$: C, 54.58; H, 3.54; N, 14.15. Found: C, 54.36; H, 3.55; N, 14.20. IR (KBr, cm^{-1}): 3649m, 3037m, 1735s, 1607m, 1514w, 1415m, 1365s, 1336s, 1240m, 1064m, 831w, 748w, 653w.

[NiMo(bimbp)$_2$O$_4$]·H$_2$O The same synthetic procedure as that for **CoMo-MOF** was used other than that the $Co(NO_3)_2 \cdot 6H_2O$ was changed to $Ni(NO_3)_2 \cdot 6H_2O$ which gave to green block of crystals in a 65% yield. Anal. calcd for $C_{36}H_{30}MoN_8NiO_5$: C, 53.38; H, 3.71; N, 13.84. Found: C, 53.22; H, 3.70; N, 13.91. IR (KBr, cm^{-1}): 3649m, 3141m, 3036m, 1735m, 1606m, 1514s, 1415m, 1365m, 1238m, 1147m, 835s, 654m.

Preparation of Co$_2$P/Mo$_3$Co$_3$C/Mo$_2$C@C and Ni/Ni$_2$P/Mo$_2$C@C

The red crystalline sample of **CoMo-MOF** and green crystalline sample of **NiMo-MOF** were put into a tube furnace with the ramping rate at 5 °C min^{-1}, subsequently, maintained at 900 °C for 4 h and naturally cooled down to 25 °C under N_2 flow. Then, the obtained black solids of **Co/Mo$_3$Co$_3$C/Mo$_2$C@C** and **Ni/Mo$_2$C@C** and NaH_2PO_2 were put at two separate positions in a porcelain boat at a ratio of 1:10, and then charged into a tube furnace with the NaH_2PO_2 at the upstream side. Then the furnace was heated to 300 °C with a heating rate of 2 °C min^{-1} for 5h. Hereafter, the samples were soaked in 2 M HCl under an ultrasonic condition for 30 min to remove the unstable compositon. Finally, copious amount of deionized water was used to wash the product until the solution is about neutral. The samples were dried at 80 °C overnight before use.

Electrochemical measurements

We use an electrochemical workstation (CHI 660e, China) to conduct the electrochemical measurements with a three-electrode system. The working electrode is a GC electrode (d = 3mm), a graphite rod is the counter electrode and the reference electrode is an Ag/AgCl electrode. For **Co$_2$P/Mo$_3$Co$_3$C/Mo$_2$C@C**, 22 mg of the samples were dispersed in the mixture of 100 μL of 0.5wt% Nafion solution, 1 mL of water and 0.8 mL of ethanol, followed by ultrasonication for 30 min to make an even suspension. After ultrasonication, 5μL of the suspension was pipetted onto the GC electrode. Then, the working electrode was dried naturally under ambient temperature. The final mass loading of the catalysts is about 0.80 mg cm^{-2}. The samples of **Ni/Ni$_2$P/Mo$_2$C@C** were prepared with the same procedure with a mass loading of 0.30 mg cm^{-2}. Commercial Pt/C electrocatalyst with same preparation was conducted with the same loading with **Co$_2$P/Mo$_3$Co$_3$C/Mo$_2$C@C**.

LSV curves were measured deaerated with nitrogen with a scan rate of 5 mV s^{-1} in 0.5 M H_2SO_4 and 1 M KOH aqueous solutions at 25 °C prior to the HER and overall water splitting measurements. And the 1 M KOH aqueous solutions was purged with O_2 prior to the OER test. The catalysts were activated using 20 cyclic voltammetry scans with a scan rate of 100 mV s^{-1} before recording the electrochemical performance. All the potentials were

referenced to a reversible hydrogen electrode (RHE) computed by the Nernst equation: $E_{RHE} = E_{Ag/AgCl} + 0.059pH + 0.197V$. All data displayed here was treated without iR compensation.

The CV measurements were taken with scan rates of 10, 30, 50, 80, 100, 150, 200 mV s^{-1} between 0.10V and 0.30V, respectively. EIS spectra were operated on a PARSTAT 2273 electrochemical system (Princeton Applied Research Instrumentation, USA) with the frequencies in the range of 0.1-100 000 Hz at an amplitude of 5 mV.

To assess the bifunctionality of **$Co_2P/Mo_3Co_3C/Mo_2C@C$** and **$Ni/Ni_2P/Mo_2C@C$** in 1 M KOH, the catalysts were loaded on two 1 x 2 cm carbon clothes (with the optimized load mass).

2. Crystal structure and physical characterization of **CoMo-MOF** and **NiMo-MOF**.

2.1 X-ray Crystallographic Analysis

X-ray single crystal data collection of **CoMo-MOF** and **NiMo-MOF** was botained on a Bruker SMART APEX II CCD diffractometer equipped with a graphite monochromator using Mo-Kα radiation (λ = 0.71073 Å) at 293 K. A multiscan technique was used to perform adsorption corrections. All the structures were solved using direct methods and refined using the full-matrix least-squares method on F^2 with anisotropic thermal parameters for all non-hydrogen atoms using the SHELXL-97 program.[1] All hydrogen atoms were located in calculated positions and refined isotropically. In the **NiMo-MOF**, free water molecules were highly disordered, and we failed to locate and refine the solvent peaks. Then, we used the SQUEEZE routine of PLATON to remove the diffused electron densities resulting from the residual solvent molecules and further refined using the data generated.[2] The final formula of **NiMo-MOF** were determined by the combination of elemental analysis, TGA data and the SQUEEZE results. The crystallographic data for **CoMo-MOF** and **NiMo-MOF** is listed in Table S1. Moreover, the selected bonds distances and bond angles are summarized in Table S2. In addition, crystallographic data of **CoMo-MOF** and **NiMo-MOF** have been deposited in Cambridge Crystallographic Data Center as supplementary publication with CCDC number: 1563105-1563106.

Reference:

(1) SHELXS-97, Sheldrick, G. M. *Acta Crystallogr. Sect. A: Found. Crystallogr.* **2008**, *64*, 112-122.

(2) Spek, A. L. *Acta Crystallogr. Sect. D: Biol. Crystallogr.* **2009**, *65*, 148-155.

Table S1. Crystallographic Data for CoMo-MOF and NiMo-MOF.

Compound	**CoMo-MOF**	**NiMo-MOF**
Chemical formula	$C_{36}H_{28}CoMoN_8O_4$	$C_{36}H_{30}MoN_8NiO_5$
Formula weigh	791.53	809.33
Crystal system	Monoclinic	Triclinic
Space group	*C2/c*	*P-1*
a (Å)	25.881(2)	12.5972(13)
b (Å)	9.9835(7)	13.8730(15)
c (Å)	13.1167(9)	14.9094(16)
α (°)	90	62.703(2)
β (°)	110.523(2)	76.533(2)
γ (°)	90	82.775(2)
V (Å^3)	3174.1(4)	2251.2(4)
Temperature (K)	293(2)	293(2)
Z	4	2
D_{calcd} (g · cm^{-3})	1.656	1.194
GOF on F^2	1.158	0.906
no. of unique data	3924	8278
no. of params refined	228	457
R_1 [$I > 2\sigma(I)$]^a	0.0303	0.0549
wR_2 [$I > 2\sigma(I)$]^b	0.0869	0.1328
$R_1{}^a$ (all data)	0.0402	0.1027
w$R_2{}^b$ (all data)	0.0911	0.1493
R_{int}	0.0289	0.0527

$^aR_1 = \sum||F_0| - |F_c||/\sum|F_0|$. $^bwR_2 = [\sum w(F_0^2 - F_c^2)^2/\sum w(F_0^2)^2]^{1/2}$

Table S2. Selected Bonds Lengths (Å) and Angles (°) for compounds CoMo-MOF

Compound **CoMo-MOF**			
Mo(1)-O(2)#1	1.7411(19)	O(2)#1-Mo(1)-O(2)	111.38(15)
Mo(1)-O(2)	1.7411(19)	O(2)#1-Mo(1)-O(1)#1	107.87(9)
Mo(1)-O(1)#1	1.7675(15)	O(2)-Mo(1)-O(1)#1	110.04(9)
Mo(1)-O(1)	1.7675(16)	O(2)#1-Mo(1)-O(1)	110.03(9)
Co(1)-O(1)#2	2.0633(16)	O(2)-Mo(1)-O(1)	107.87(9)
Co(1)-O(1)	2.0633(16)	O(1)#1-Mo(1)-O(1)	109.65(11)
Co(1)-N(4)#3	2.1623(19)	O(1)#2-Co(1)-O(1)	180
Co(1)-N(4)#4	2.1623(19)	O(1)#2-Co(1)-N(4)#3	91.11(7)
Co(1)-N(1)	2.1913(19)	O(1)-Co(1)-N(4)#3	88.89(7)
Co(1)-N(1)#2	2.1913(19)	O(1)#2-Co(1)-N(4)#4	88.89(7)
O(1)-Co(1)-N(4)#4	91.11(7)	O(1)#2-Co(1)-N(1)#2	87.38(7)
N(4)#3-Co(1)-N(4)#4	180.00(4)	O(1)-Co(1)-N(1)#2	92.62(7)
O(1)#2-Co(1)-N(1)	92.62(7)	N(4)#3-Co(1)-N(1)#2	83.17(8)
O(1)-Co(1)-N(1)	87.38(7)	N(4)#4-Co(1)-N(1)#2	96.83(8)
N(4)#3-Co(1)-N(1)	96.83(8)	N(1)-Co(1)-N(1)#2	180
N(4)#4-Co(1)-N(1)	83.17(8)		

Symmetry codes: for compound **CoMo-MOF**: #1 –x + 1, y, -z + 1/2; #2 –x + 1, -y + 1, -z; #3 x + 1/2, -y + 3/2, z - 1/2; #4 –x + 1/2, y - 1/2, -z + 1/2; #5 –x + 1/2, y + 1/2, -z + 1/2.

Table S3. Selected Bonds Lengths (Å) and Angles (°) for compounds NiMo-MOF

Compound **NiMo-MOF**			
Ni(1)-O(4)#1	1.95(2)	N(4)#3-Ni(1)-N(4)#4	172.0(7)
Ni(1)-N(8)#2	1.993(18)	O(4)-Ni(1)-N(4)#4	86.9(7)
Ni(1)-N(4)#3	2.076(18)	Ni(1)#1-Ni(1)-N(8)#5	35(8)
Ni(1)-O(4)	2.110(19)	O(4)#1-Ni(1)-N(8)#5	88.7(9)
Ni(1)-N(4)#4	2.154(18)	N(8)#2-Ni(1)-N(8)#5	174.9(10)
Ni(1)-N(8)#5	2.236(17)	N(4)#3-Ni(1)-N(8)#5	84.6(6)
Ni(2)-O(1)	2.026(3)	O(4)-Ni(1)-N(8)#5	84.4(5)
Ni(2)-O(1)#6	2.026(3)	N(4)#4-Ni(1)-N(8)#5	88.6(6)
Ni(2)-N(5)	2.099(4)	O(1)-Ni(2)-O(1)#6	180
Ni(2)-N(5)#6	2.099(4)	O(1)-Ni(2)-N(5)	90.04(16)
Ni(2)-N(1)	2.113(4)	O(1)#6-Ni(2)-N(5)	89.96(16)
Ni(2)-N(1)#6	2.113(4)	O(1)-Ni(2)-N(5)#6	89.96(16)
Mo(1)-O(2)	1.725(4)	O(1)#6-Ni(2)-N(5)#6	90.04(16)
Mo(1)-O(4)	1.746(4)	N(5)-Ni(2)-N(5)#6	180
Mo(1)-O(1)	1.759(3)	O(1)-Ni(2)-N(1)	90.37(16)
Mo(1)-O(3)	1.766(4)	O(1)#6-Ni(2)-N(1)	89.63(16)
O(4)#1-Ni(1)-N(8)#2	95.6(6)	N(5)-Ni(2)-N(1)	93.37(17)
Ni(1)#1-Ni(1)-N(4)#3	101(7)	N(5)#6-Ni(2)-N(1)	86.63(17)
O(4)#1-Ni(1)-N(4)#3	93.5(8)	O(1)-Ni(2)-N(1)#6	89.63(16)
N(8)#2-Ni(1)-N(4)#3	97.8(7)	O(1)#6-Ni(2)-N(1)#6	90.37(16)
Ni(1)#1-Ni(1)-O(4)	54(8)	N(5)-Ni(2)-N(1)#6	86.63(17)
O(4)#1-Ni(1)-O(4)	172.6(9)	N(5)#6-Ni(2)-N(1)#6	93.37(17)
N(8)#2-Ni(1)-O(4)	91.2(9)	N(1)-Ni(2)-N(1)#6	180
N(4)#3-Ni(1)-O(4)	88.3(7)	O(2)-Mo(1)-O(4)	108.6(2)
Ni(1)#1-Ni(1)-N(4)#4	71(7)	O(2)-Mo(1)-O(1)	109.5(2)
O(4)#1-Ni(1)-N(4)#4	90.5(8)	O(4)-Mo(1)-O(1)	109.08(18)
N(8)#2-Ni(1)-N(4)#4	88.8(7)	O(2)-Mo(1)-O(3)	111.6(3)
O(4)-Mo(1)-O(3)	109.2(2)	O(1)-Mo(1)-O(3)	108.8(2)

Symmetry codes: for compound **NiMo-MOF**: #1 –x + 2, -y + 1, -z + 1; #2 x, y + 1, z – 1; #3 x + 1, y, z + 1; #4 –x + 1, -y + 1, -z; #5 –x + 2, -y, -z + 2; #6 –x + 1, -y + 1, -z + 1.

2.2 **Structure of compound CoMo-MOF and NiMo-MOF.**

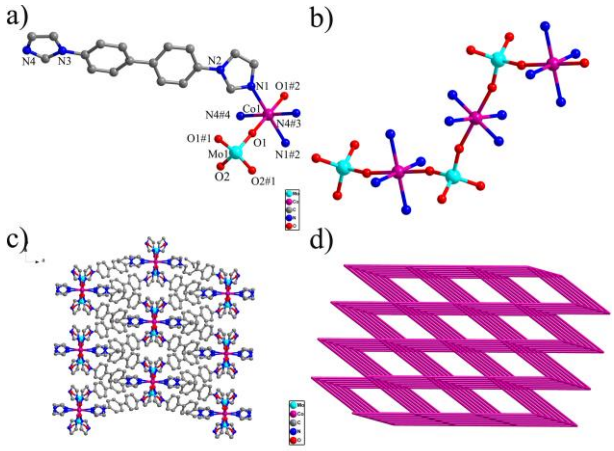

Fig. S1 (a) Co(II) coordination environments of **CoMo-MOF**. (b) 1D chain of **CoMo-MOF**. (c) 3D framework of **CoMo-MOF.** (d) 3D uninodal 6-connected pcu net with a (4^{12}•6^3) topology of **CoMo-MOF**. All hydrogen atoms are omitted for clarity.

X-ray determination has revealed that **CoMo-MOF** crystalized in the monoclinic system with C2/c space group. The asymmetric unit includes one Co (II) ion, one Mo (VI) ion and one bimbp ligand are shown in Figure S1a. Co1 adpots a hexacoordinated octahedral fashion geometry by connecting to two oxygen atoms and four nitrogen atoms from two bpp ligands. The average Co-O and Co-N distances are 2.026(4) Å and from 2.1623(19) to 2.1913(19) Å, respectively. Mo1 shows MoO_4 tetrahedron coordination configuration, and each molybdenum centre is coordinated with two bridging oxygen atoms (O_b) and two terminal oxygen atoms (O_t). The Mo-O_t distance of 1.7411(19) Å is slightly shorter than the Mo-O_b distances of 1.7675(16) Å. The Co ions and adjacent Mo ions are connected through the bridging oxygen atoms to form a one dimensional chain, displayed in Fig S1b. Then, the one dimensional chains are further linked by bimbp ligands to assemble into a 3D framework (Fig. S1c). Topologically, **CoMo-MOF** is a uninodal 6-connected net with the Schäfli symbol of {4^{12}•6^3} as depicted in Figure. S3d.

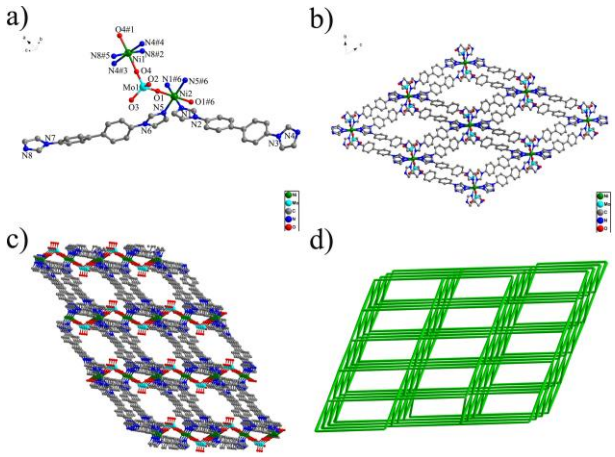

Fig. S2 (a) Ni(II) coordination environments of **NiMo-MOF**. (b) and (c) 3D framework of **NiMo-MOF** with 1D channels running along *a* and *c* axes. (d) 3D uninodal 6-connected pcu net with a (4^{12}•6^3) topology of **NiMo-MOF**. All hydrogen atoms are omitted for clarity.

X-ray determination has revealed that **NiMo-MOF** crystalized in the triclinic system with P-*1* space group. The asymmetric unit includes two halves Ni (II) ions, one Mo (VI) ion and two bimbp ligands are shown in Figure S2a. Both Ni1 and Ni2 adpot a hexacoordinated octahedral fashion geometry by connecting to two oxygen atoms and four nitrogen atoms from two bpp ligands. The average Ni-O and Ni-N distances are from 1.95(2) to 2.110(19)Å and from 1.993(18) to 2.113(4) Å , respectively. Mo1 shows MoO_4 tetrahedron coordination configuration, and each molybdenum centre is coordinated with two bridging oxygen atoms (O_b) and two terminal oxygen atoms (O_t). The Mo-O_t distances are 1.725(4) and 1.766(4) Å and the Mo-O_b distances are 1.746(4) and 1.759(3) Å. The Ni ions and adjacent Mo ions are connected through the bridging oxygen atoms to form a one dimensional chain. Then, the one dimensional chains are further linked by bimbp ligands to assemble into a 3D framework with 1D channels along *a* and *c* axes (Fig. S2b and S2c). There exist one dimensional channels along a and b axes. Topologically, **NiMo-MOF** is a uninodal 6-connected net with the Schäfli symbol of {4^{12}•6^3} as depicted in Figure. S2d.

3. Physical characterization of **CoMo-MOF** and **NiMo-MOF**.

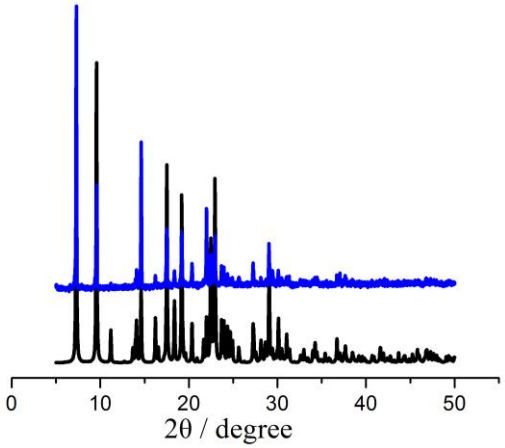

Fig. S3 Experimental (blue), simulated (black) PXRD patterns for compound **CoMo-MOF**.

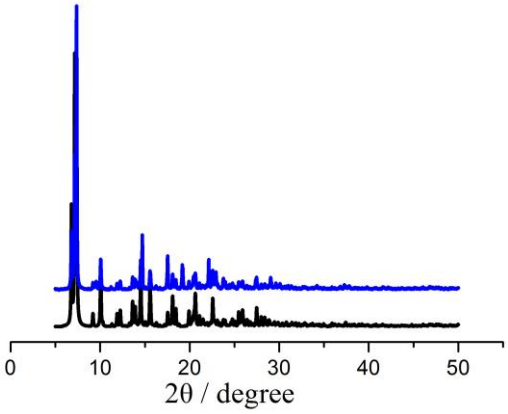

Fig. S4 Experimental (blue), simulated (black) PXRD patterns for compound **NiMo-MOF**.

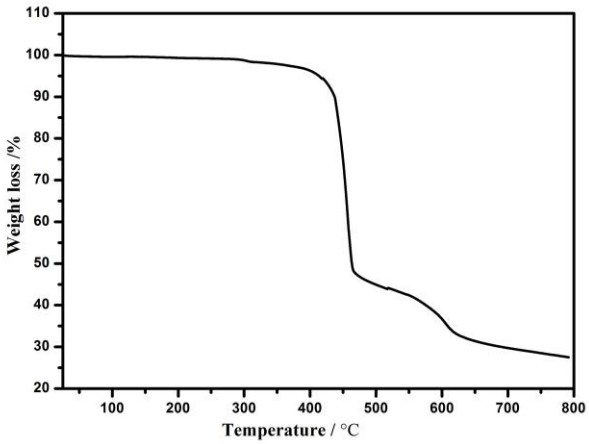

Fig. S5 The TGA curves for compound **CoMo-MOF**.

To study the thermal stabilities of **CoMo-MOF**, the thermogravimetric analyses were carried out under N_2 atmosphere from room temperature to 800 °C with a heating rate of 10 °C min^{-1}. **CoMo-MOF** can be stable up to 400 °C, shown in Fig. S5. Then with the increase of temperature, the framework collapsed and decomposed. The residues are CoO and MoO_3 (experimental: 27.51% and calculated 27.65%).

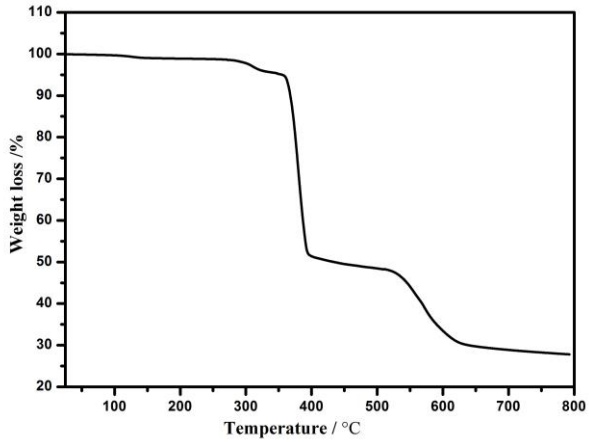

Fig. S6 The TGA curves for compound Ni**Mo-MOF**.

To study the thermal stabilities of **NiMo-MOF**, the thermogravimetric analyses were carried out under N_2 atmosphere from room temperature to 800 °C with a heating rate of 10 °C min^{-1}. **NiMo-MOF** shows a slow weight loss of 2.33% before 300 °C, which corresponds to the loss of solvent water molecules (calculated 2.25%). Then with the increase of temperature, the framework collapsed and decomposed. The residues are NiO and MoO_3 (experimental: 27.76% and calculated 27.28%).

4. Physical characterization of **$Co_2P/Mo_3Co_3C/Mo_2C@C$** and **$Ni/Ni_2P/Mo_2C@C$**.

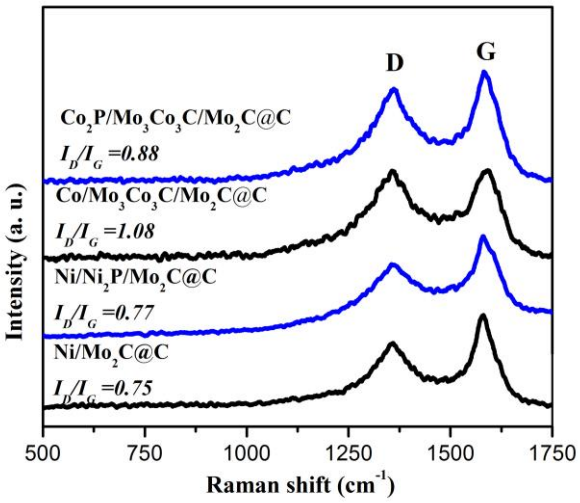

Fig. S7 Raman spectra of **$Co_2P/Mo_3Co_3C/Mo_2C@C$**, **$Co/Mo_3Co_3C/Mo_2C@C$**, **$Ni/Ni_2P/Mo_2C@C$** and **$Ni/Mo_2C@C$**.

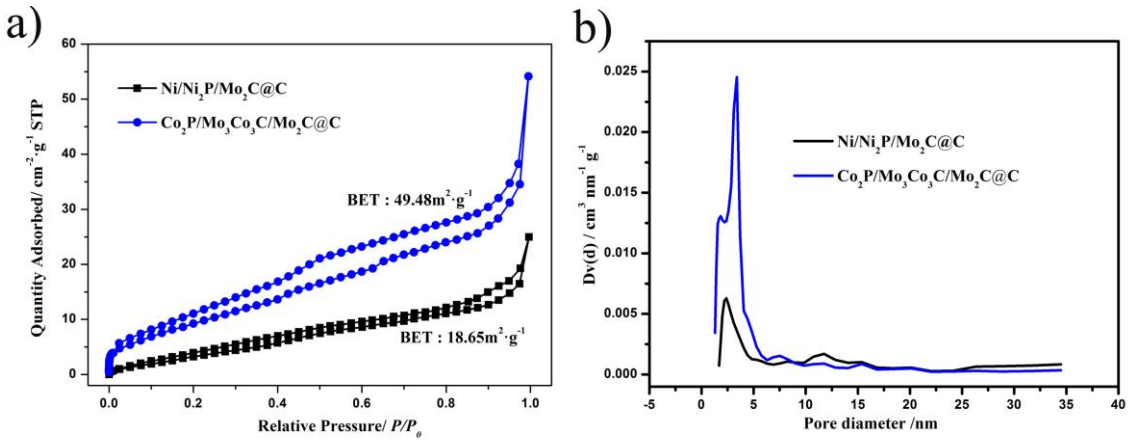

Fig. S8 (a) N_2 adsorption-desorption isotherms. (b) The pore-size distribution of **$Co_2P/Mo_3Co_3C/Mo_2C@C$** and **$Ni/Ni_2P/Mo_2C@C$**.

5. Additional electrochemical experiments of **$Co_2P/Mo_3Co_3C/Mo_2C$@C** and **Ni/Ni_2P/Mo_2C@C**.

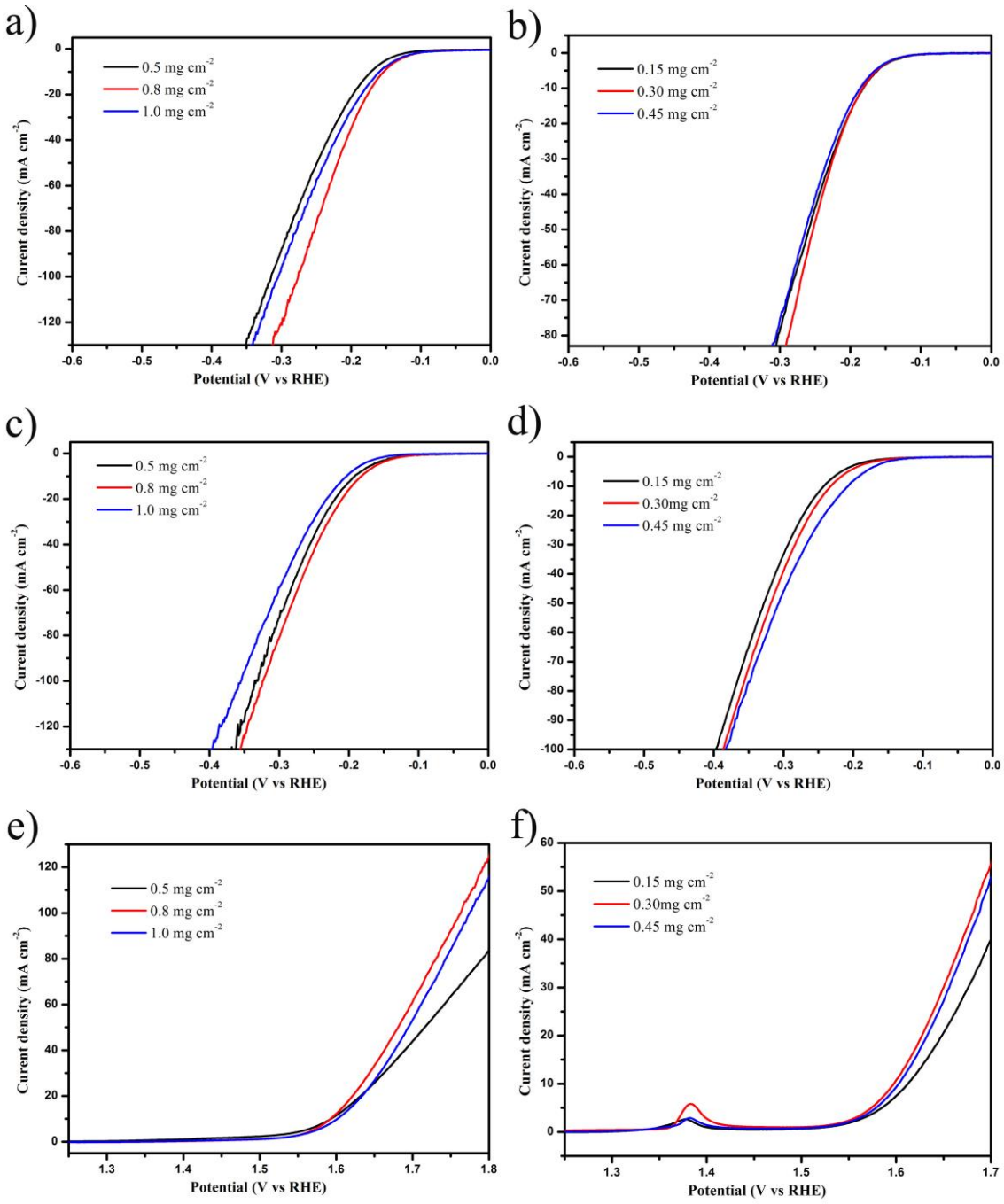

Fig. S9 (a) and (b) HER polarization curves of **$Co_2P/Mo_3Co_3C/Mo_2C$@C** and **Ni/Ni_2P/Mo_2C@C** with different mass loadings on a glassy carbon electrode in 0.5 M H_2SO_4, (c) and (d) HER polarization curves in 1 M KOH, (e) and (f) OER polarization curves in 1 M KOH.

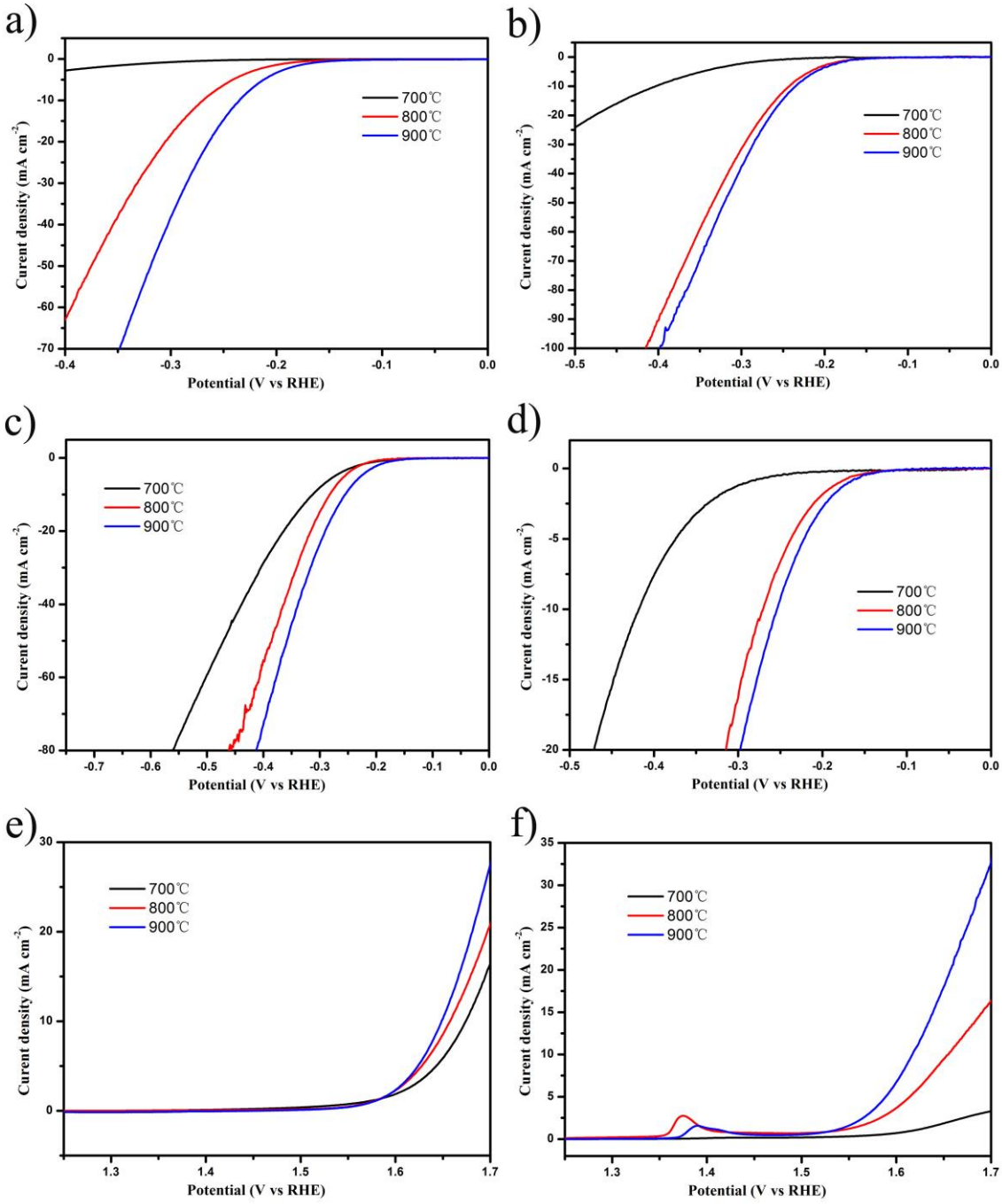

Fig. S10 (a) and (b) HER polarization curves of **$Co_2P/Mo_3Co_3C/Mo_2C$@C** and **$Ni/Ni_2P/Mo_2C$@C** with different carburization temperature for two hours on a glassy carbon electrode in 0.5 M H_2SO_4, (c) and (d) HER polarization curves in 1 M KOH, (e) and (f) OER polarization curves in 1 M KOH.

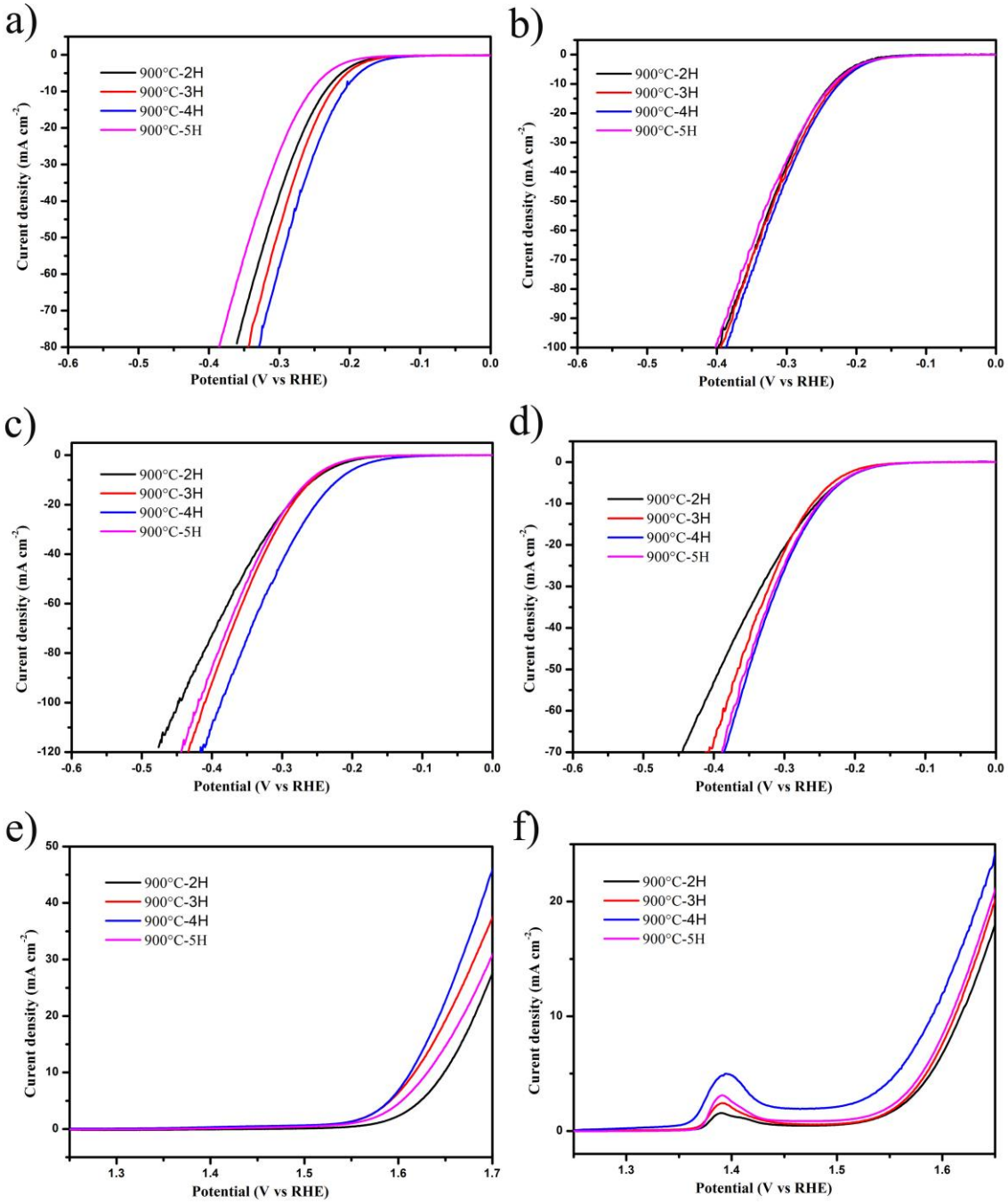

Fig. S11 (a) and (b) HER polarization curves of **$Co_2P/Mo_3Co_3C/Mo_2C$@C** and **$Ni/Ni_2P/Mo_2C$@C** with different carburization time on a glassy carbon electrode in 0.5 M H_2SO_4, (c) and (d) HER polarization curves in 1 M KOH, (e) and (f) OER polarization curves in 1 M KOH.

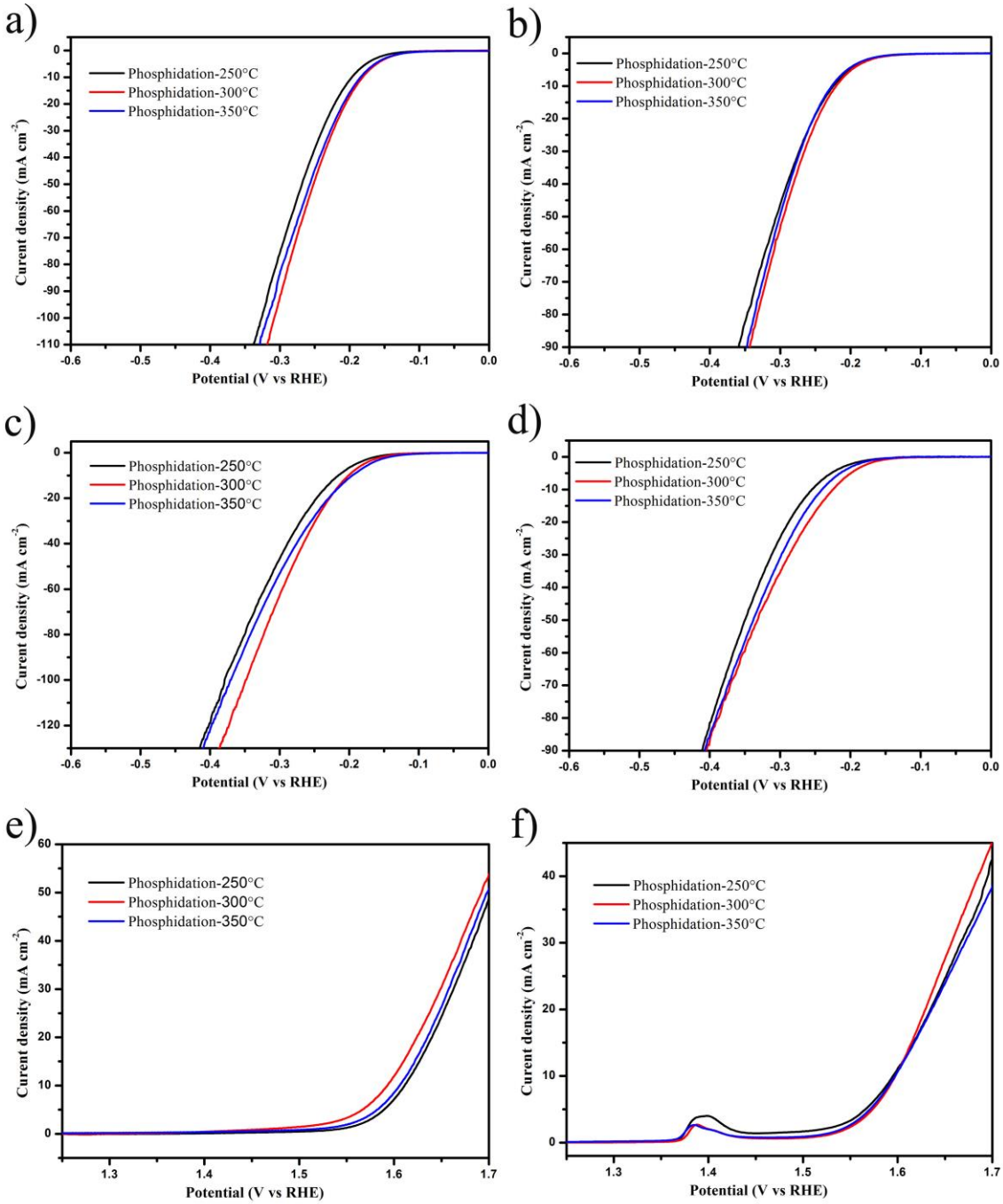

Fig. S12 (a) and (b) HER polarization curves of **$Co_2P/Mo_3Co_3C/Mo_2C$@C** and **$Ni/Ni_2P/Mo_2C$@C** with different phosphidation temperature for two hours on a glassy carbon electrode in 0.5 M H_2SO_4, (c) and (d) HER polarization curves in 1 M KOH, (e) and (f) OER polarization curves in 1 M KOH.

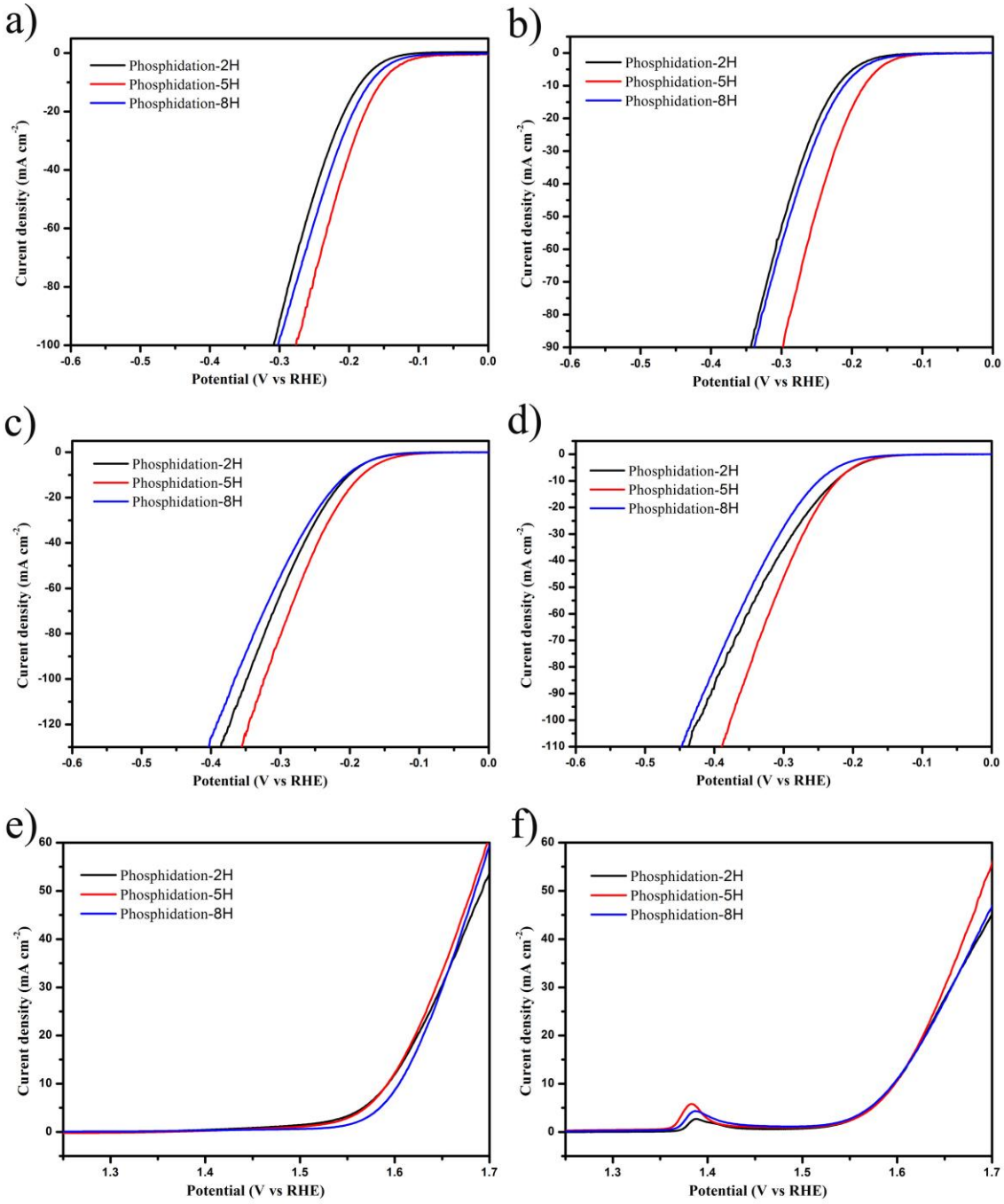

Fig. S13 (a) and (b) HER polarization curves of **$Co_2P/Mo_3Co_3C/Mo_2C$@C** and **$Ni/Ni_2P/Mo_2C$@C** with different phosphidation time at 300 °C on a glassy carbon electrode in 0.5 M H_2SO_4, (c) and (d) HER polarization curves in 1 M KOH, (e) and (f) OER polarization curves in 1 M KOH.

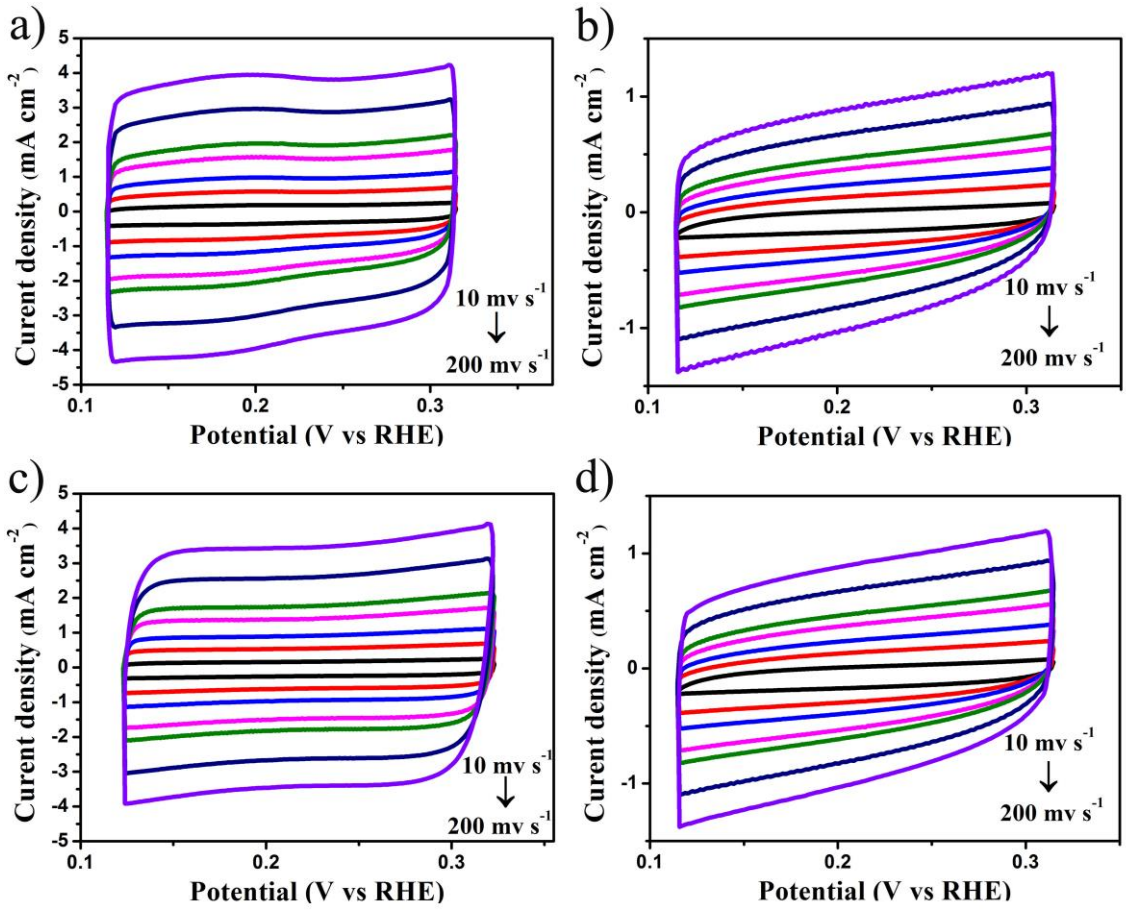

Fig. S14 Cyclic voltammograms (CVs) of **$Co_2P/Mo_3Co_3C/Mo_2C@C$** and **$Ni/Ni_2P/Mo_2C@C$** in 0.5 M H_2SO_4 (a-b) and 1 M KOH (c-d).

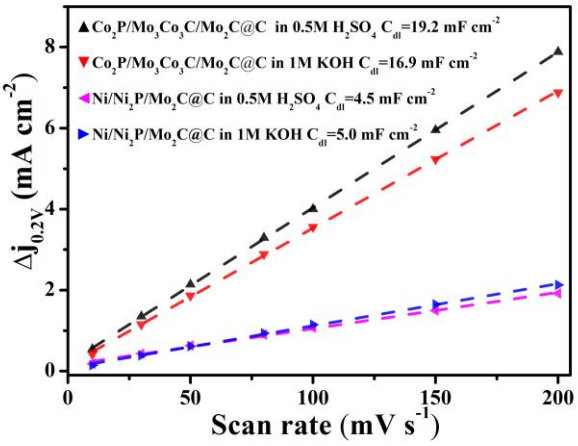

Fig. S15 Liner fitting of Δ_j ($\Delta_j = j_a - j_c$) vs. scan rates at a given overpotential of + 0.2V vs. RHE in 0.5 M H_2SO_4 and in 1 M KOH, respectively. j_a represents the anodic current density and j_c represents the cathodic current density.

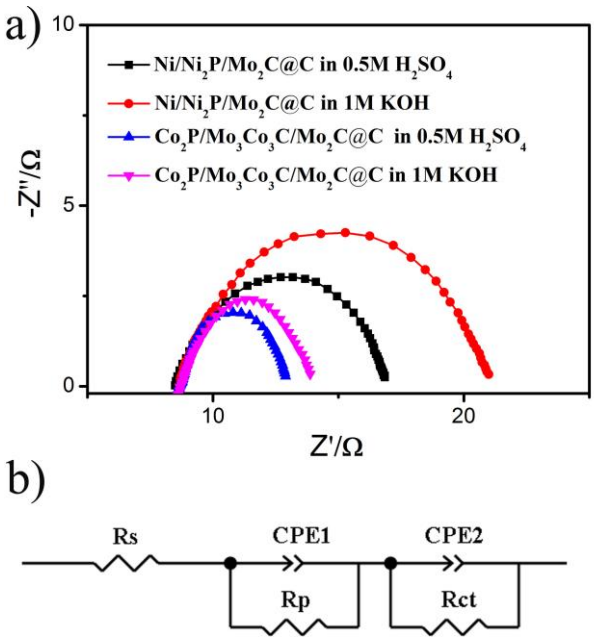

Fig. S16 (a) Nyquist plots of electrochemical impedance spectra (EIS) of **$Co_2P/Mo_3Co_3C/Mo_2C$@C** and **$Ni/Ni_2P/Mo_2C$@C** obtained in 0.5 M H_2SO_4 and 1 M KOH aqueous solutions at an overpotential of 100 mV. (b) Two-time constant model, including a series resistance (R_s), two constant phase elements (CPE1 and CPE2), resistance corresponding to surface porosity (R_p), and charge transfer resistance corresponding to HER process (R_{ct}).

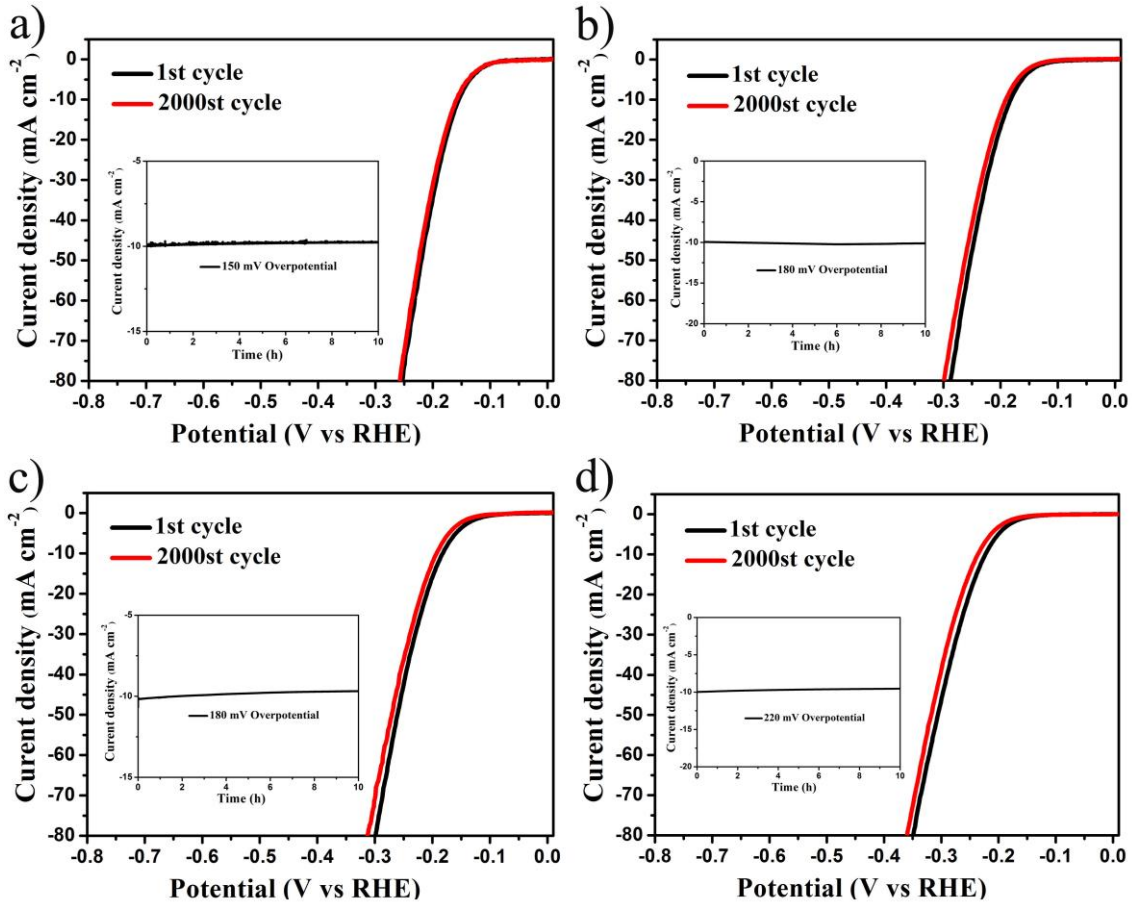

Fig. S17 Polarization curves of **$Co_2P/Mo_3Co_3C/Mo_2C$@C** and **$Ni/Ni_2P/Mo_2C$@C** for HER activities after continuous potential sweeps at 50 mV s^{-1} in 0.5 M H_2SO_4 (a – b) and 1 M KOH (c - d). Insets: time - dependent durrent density cureves under static overpotentials.

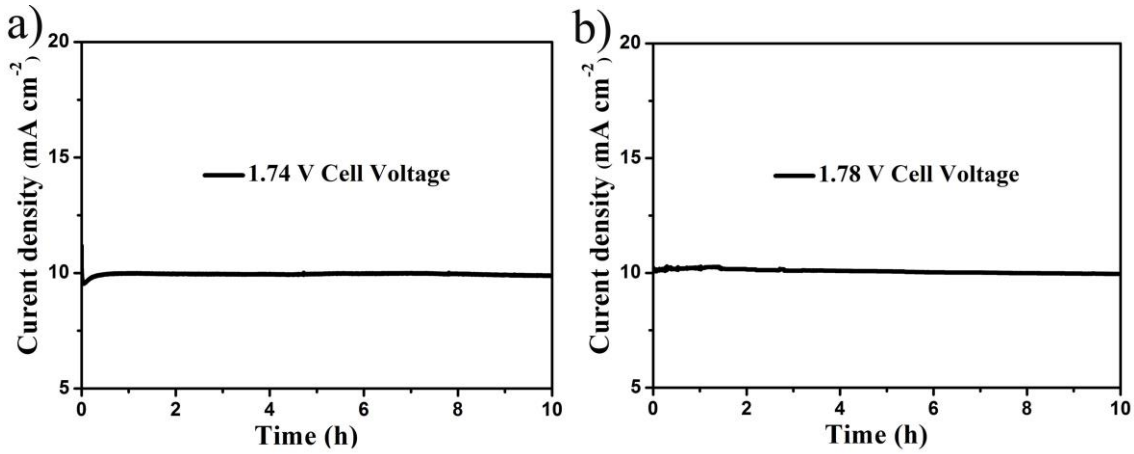

Fig. S18 (a) and (b) The stability of **$Co_2P/Mo_3Co_3C/Mo_2C$@C** and **$Ni/Ni_2P/Mo_2C$@C** for water splitting at an applied voltage for 10 h. The loadings of both cathode and anode are the optimized mass loadings.

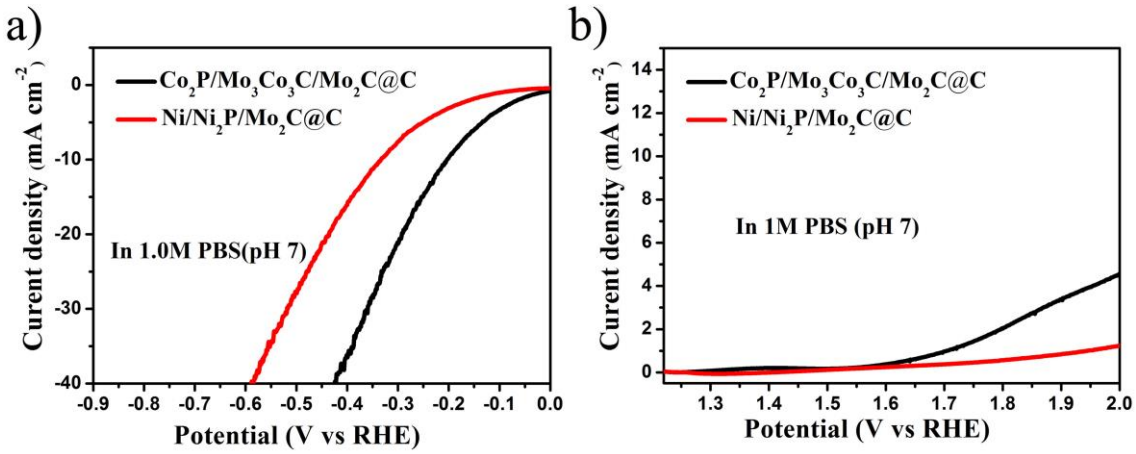

Fig. S19 (a) and (b) HER and OER polarization curves of **$Co_2P/Mo_3Co_3C/Mo_2C$@C** and **$Ni/Ni_2P/Mo_2C$@C** in neutral electrolytes. The loadings of both catalysts are the optimized mass loadings.

Note: The **$Co_2P/Mo_3Co_3C/Mo_2C$@C** and **$Ni/Ni_2P/Mo_2C$@C** catalysed HER efficiently in neutral conditions, which needed overpotentials of 204 and 334 mV to reach a current density of 10 mA cm^{-2}, respectively. However, the catalysts show poor results for OER in neutral electrolytes, which were much worse than those in basic solutions. These results are consistent with most non-noble metal catalysts reported in the literatures which exhibit good HER activity at wide pH values while remarkable OER performance only in alkaline electrolytes.

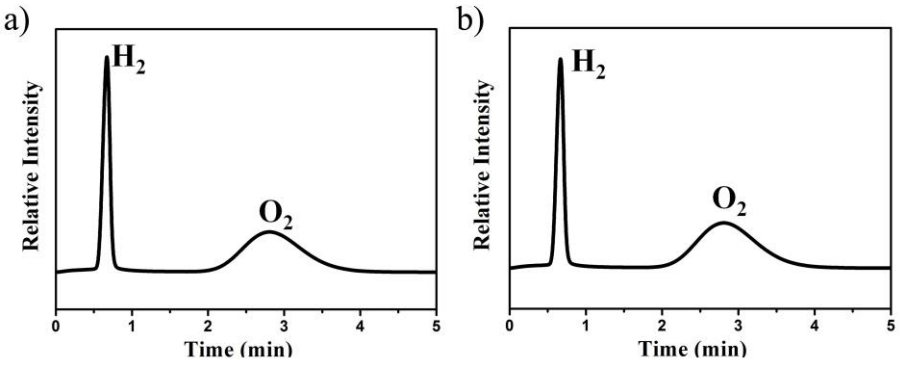

Fig.S20 (a) and (b) Gas chromatogram of the evolved hydrogen and oxygen during the electrocatalytic water splitting of **$Co_2P/Mo_2C/Mo_3Co_3C$@C** and **$Ni/Ni_2P/Mo_2C$@C**.

Note: only H_2 and O_2 were detected, which confirms the water splitting.

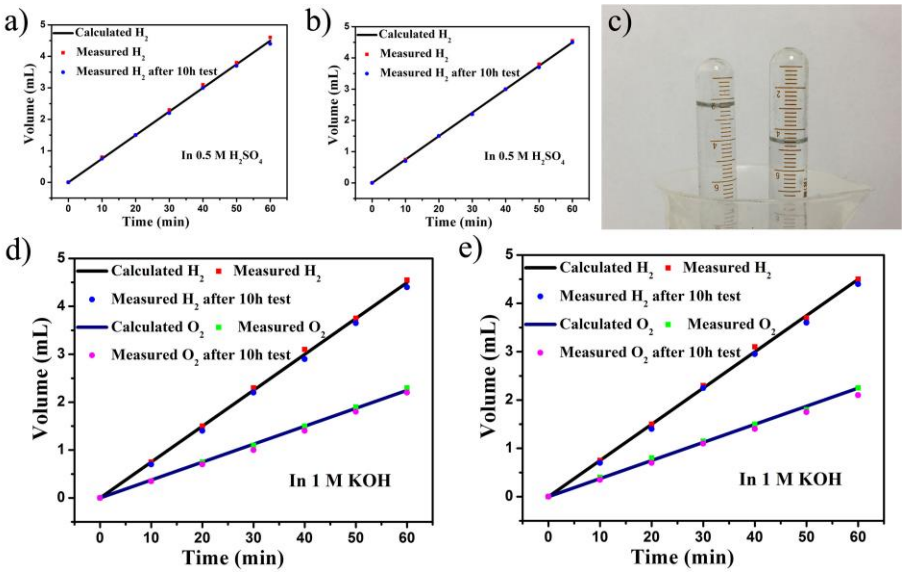

Fig.S21 (a) and (b) The comparison between the theoretical amount of H_2 calculated from a chronopotentiometric response at 10 $mA \cdot cm^{-2}$ and the measured amount of H_2 experimentally showing Faradaic efficiency of HER before and after 10 h test for the **$Co_2P/Mo_2C/Mo_3Co_3C$@C** and **$Ni/Ni_2P/Mo_2C$@C** in 0.5 M H_2SO_4; (c) The optical image Oxygen and hydrogen collection process with displacement of water; (e) and (f) the Faradaic efficiency of H_2 and O_2 before and after 10 h test for the **$Co_2P/Mo_2C/Mo_3Co_3C$@C** and **$Ni/Ni_2P/Mo_2C$@C** in 1 M KOH.

Note: H_2 and O_2 were collected by drainage collection methods. Both **$Co_2P/Mo_2C/Mo_3Co_3C$@C** and **$Ni/Ni_2P/Mo_2C$@C** were limited to chronopotentiometric response at a current of 10 mA. Fig. S20a and S20b show the Faradaic efficiency of **$Co_2P/Mo_2C/Mo_3Co_3C$@C** and **$Ni/Ni_2P/Mo_2C$@C** was nearly 100% for HER in 0.5 M H_2SO_4, and after 10 h-running, the Faradaic efficiency for both electrocatalysts retained ~ 100%. Thus, both of the electrocatalysts were considered to be valuable and stable electrocatalysts for HER. In 1 M KOH, two-electrode setup was used for measuring the Faradaic efficiency of H_2 and O_2. The results (Fig. S20c-S20e) showed the Faradaic efficiency for both **$Co_2P/Mo_2C/Mo_3Co_3C$@C** and **$Ni/Ni_2P/Mo_2C$@C** was nearly 100% for overall water splitting. After 10 h test, the Faradaic efficiency of H_2 and O_2 for both electrocatalysts remained almost 100%, which can be believed that both the both **$Co_2P/Mo_2C/Mo_3Co_3C$@C** and **$Ni/Ni_2P/Mo_2C$@C** have robust stability with high activity under long-time operation in alkaline conditions.

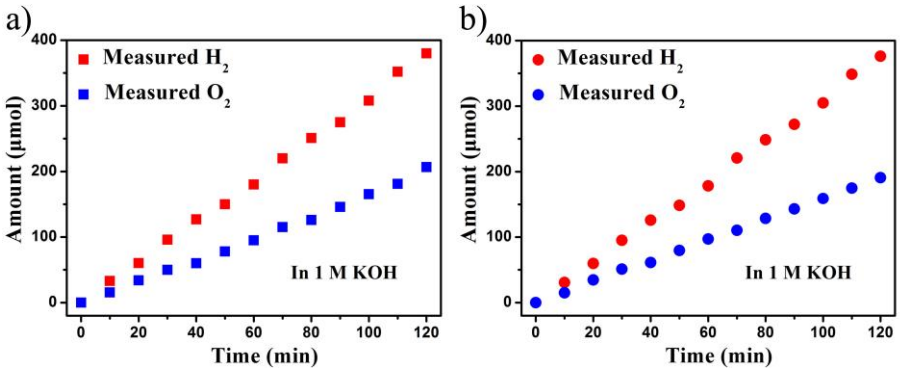

Fig.S22 (a) and (b) The measured amount of H_2 and O_2 experimentally at 10 mA·cm^{-2} for 120 min by on-line gas chromatography for the **$Co_2P/Mo_2C/Mo_3Co_3C$@C** and **$Ni/Ni_2P/Mo_2C$@C**.

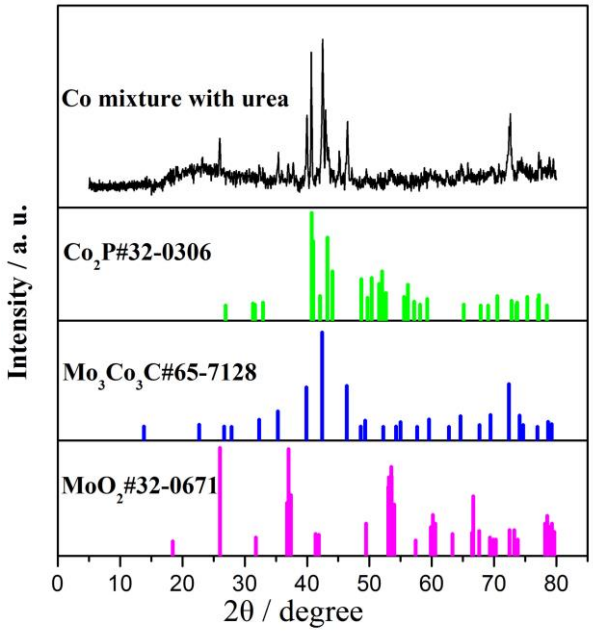

Fig. S23 PXRD patterns for Co mixture with urea.

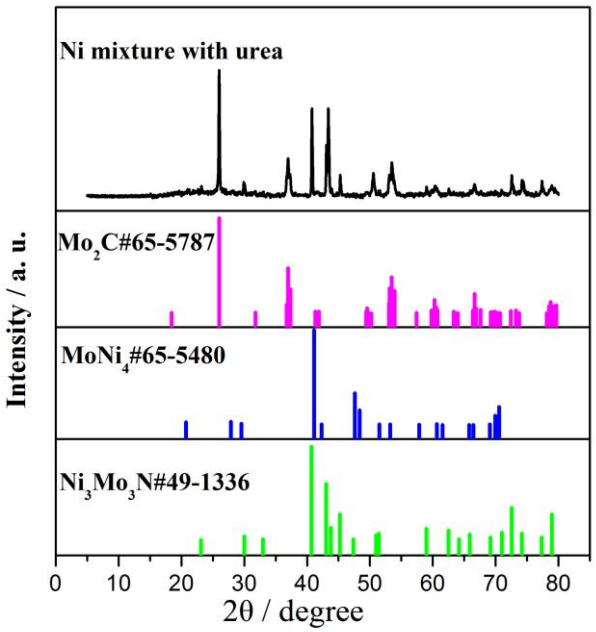

Fig. S24 PXRD patterns for Ni mixture with urea.

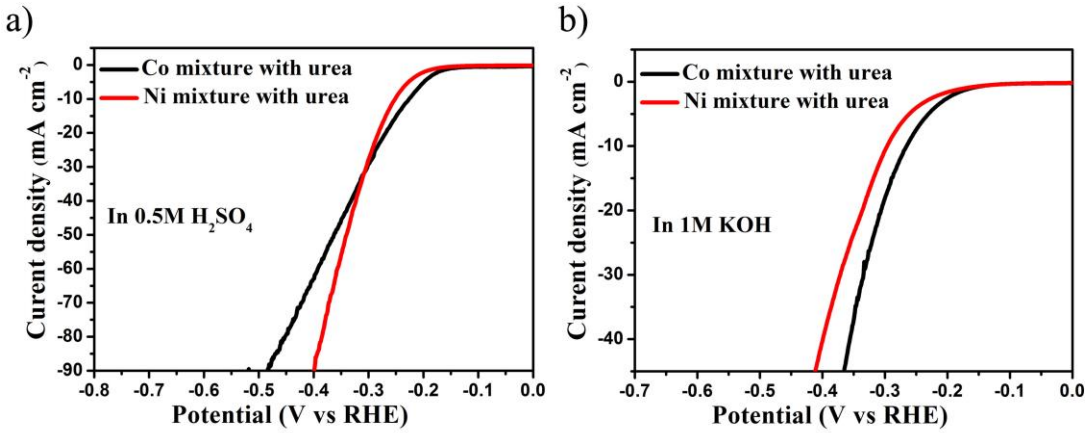

Fig. S25 (a) and (b) HER polarization curves of Co mixture with urea and Ni mixture with urea in acid and basic electrolytes. The loadings of both catalysts are the optimized mass loadings.

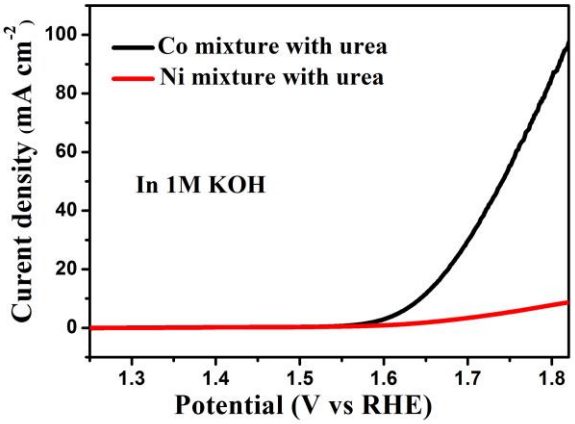

Fig. S26 OER polarization curves of Co mixture with urea and Ni mixture with urea in basic electrolytes. The loadings of both catalysts are the optimized mass loadings.

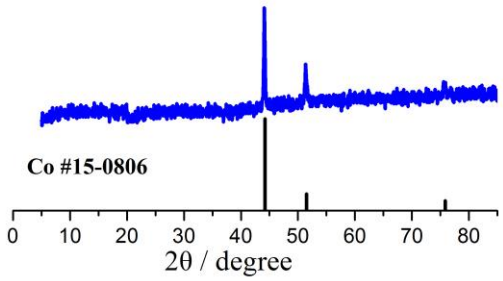

Fig. S27 PXRD patterns for Co mixed with bimbp-precursor after 900 °C for 4 h.

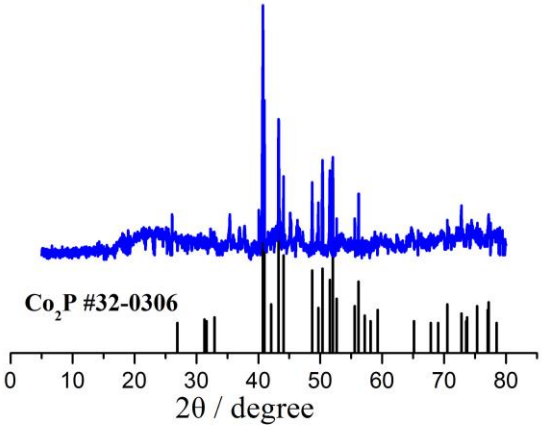

Fig. S28 PXRD patterns for Co mixed with bimbp-precursor after 900 °C for 4 h and following phosphidation.

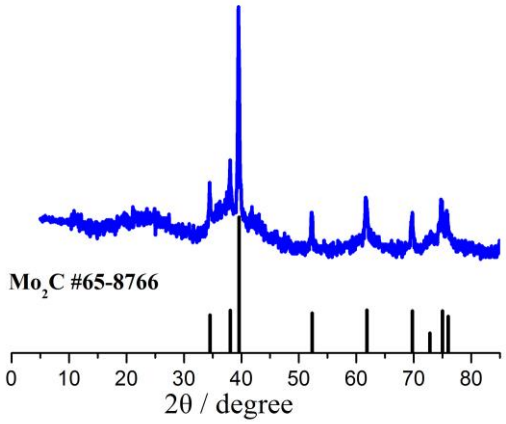

Fig. S29 PXRD patterns for Mo mixed with bimbp-precursor after 900 °C for 4 h and following phosphidation.

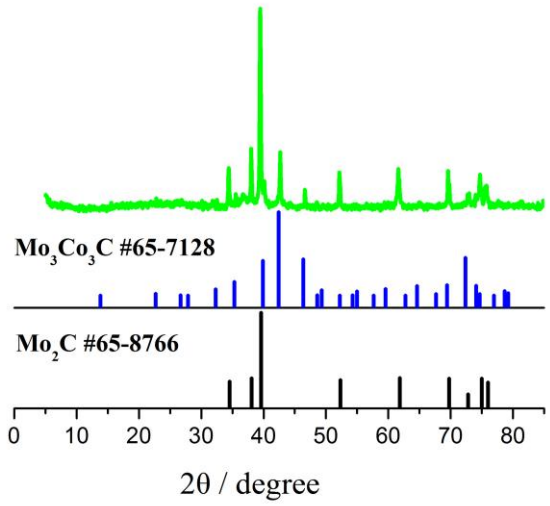

Fig. S30 PXRD patterns for Co and Mo mixed with bimbp-precursor after 900 °C for 4 h and following phosphidation.

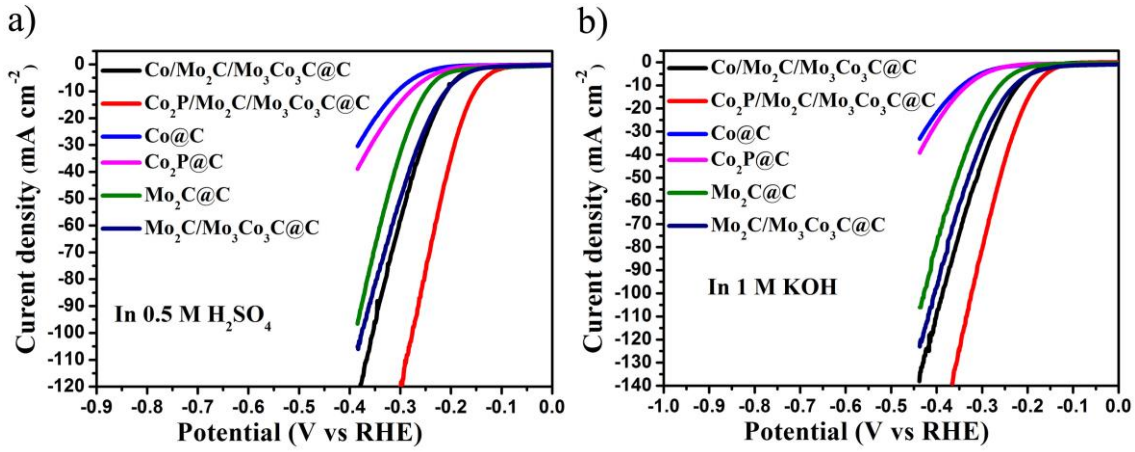

Fig. S31 (a) and (b) HER polarization curves of in acid and basic electrolytes. The loadings of all catalysts are the optimized mass loadings.

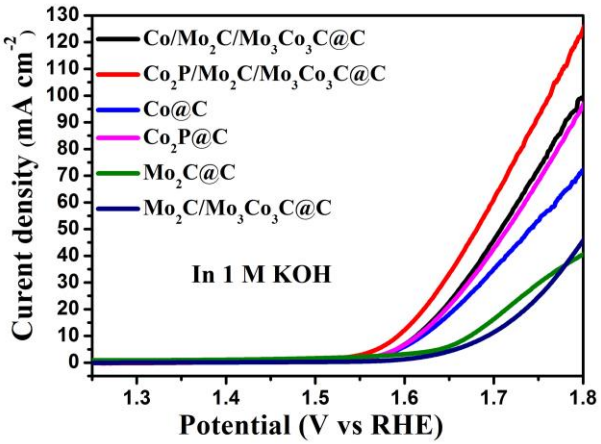

Fig. S32 OER polarization curves in basic electrolytes. The loadings of all catalysts are the optimized mass loadings.

6. XPS spectra of **Co/Mo_3Co_3C/Mo_2C@C, $Co_2P/Mo_3Co_3C/Mo_2C$@C, Ni/Mo_2C@C** and **Ni/Ni_2P/Mo_2C@C** before and after electrochemical tests.

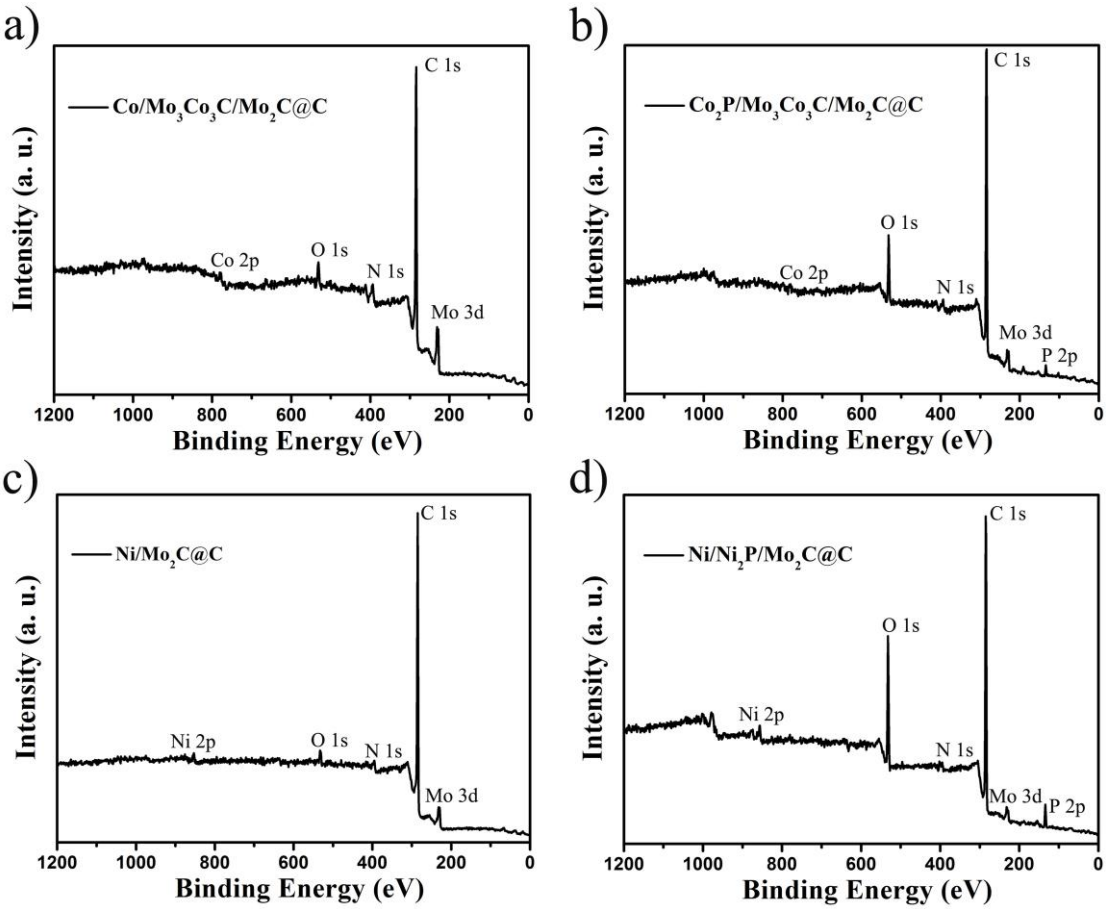

Fig. S33 (a) - (d) X-ray photoelectron spectra of **Co/Mo_3Co_3C/Mo_2C@C**, **$Co_2P/Mo_3Co_3C/Mo_2C$@C**, **Ni/Mo_2C@C** and **Ni/Ni_2P/Mo_2C@C**, confirming the presence of P in **$Co_2P/Mo_3Co_3C/Mo_2C$@C** and **Ni/Ni_2P/Mo_2C@C**.

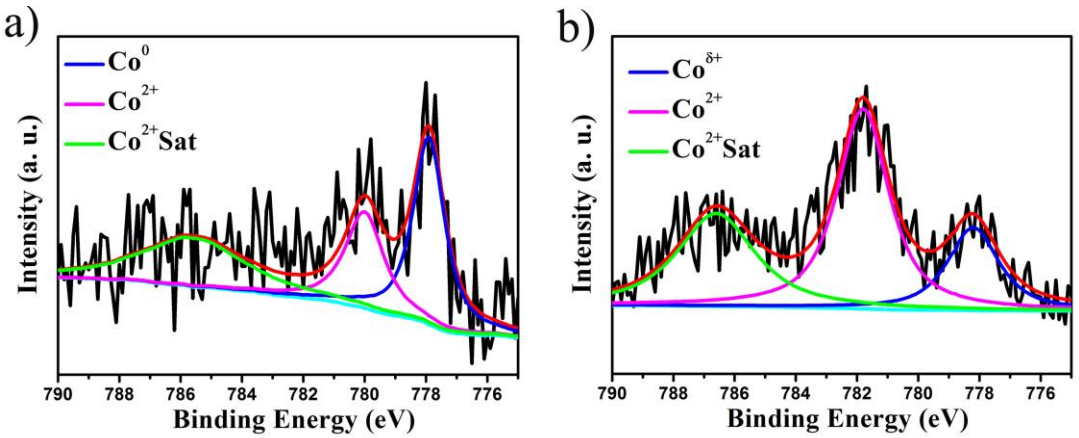

Fig. S34 (a)-(b) The high resolution Co 2p XPS of **Co/Mo$_3$Co$_3$C/Mo$_2$C@C and Co$_2$P/Mo$_3$Co$_3$C/Mo$_2$C@C**.

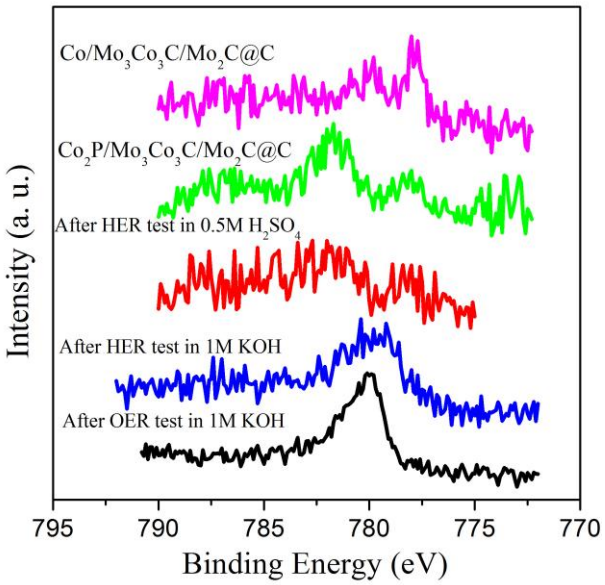

Fig. S35 The high resolution Co 2p XPS of **Co$_2$P/Mo$_3$Co$_3$C/Mo$_2$C@C** before and after HER and OER tests.

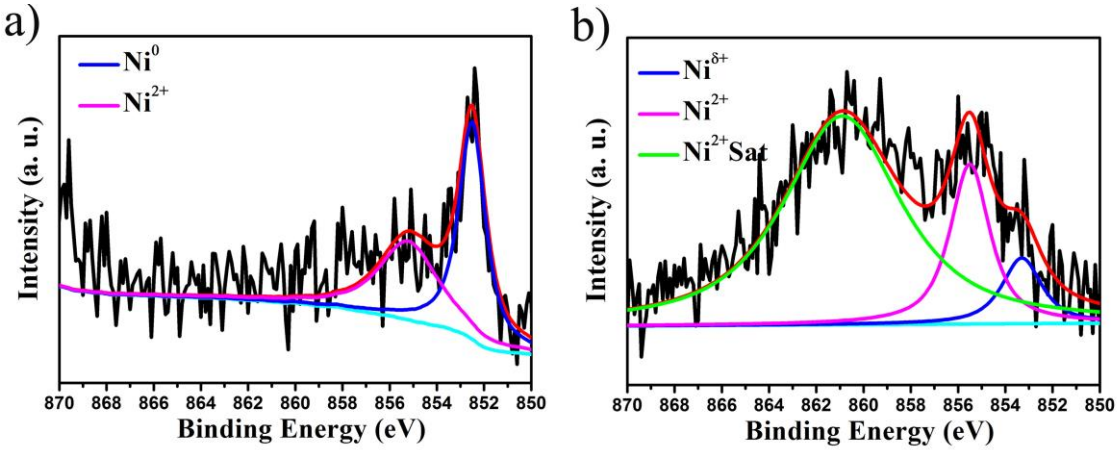

Fig. S36 (a)-(b) The high resolution Ni 2p XPS of **Ni/Mo$_2$C@C** and **Ni/Ni$_2$P/Mo$_2$C@C**.

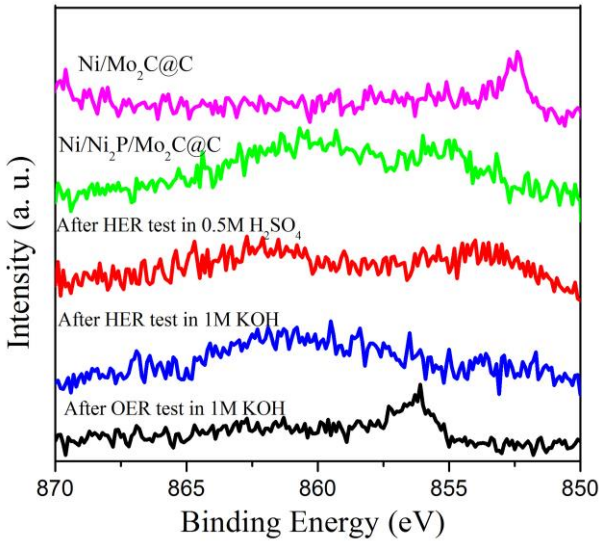

Fig. S37 The high resolution Ni 2p XPS of **Ni/Ni$_2$P/Mo$_2$C@C** before and after HER and OER tests.

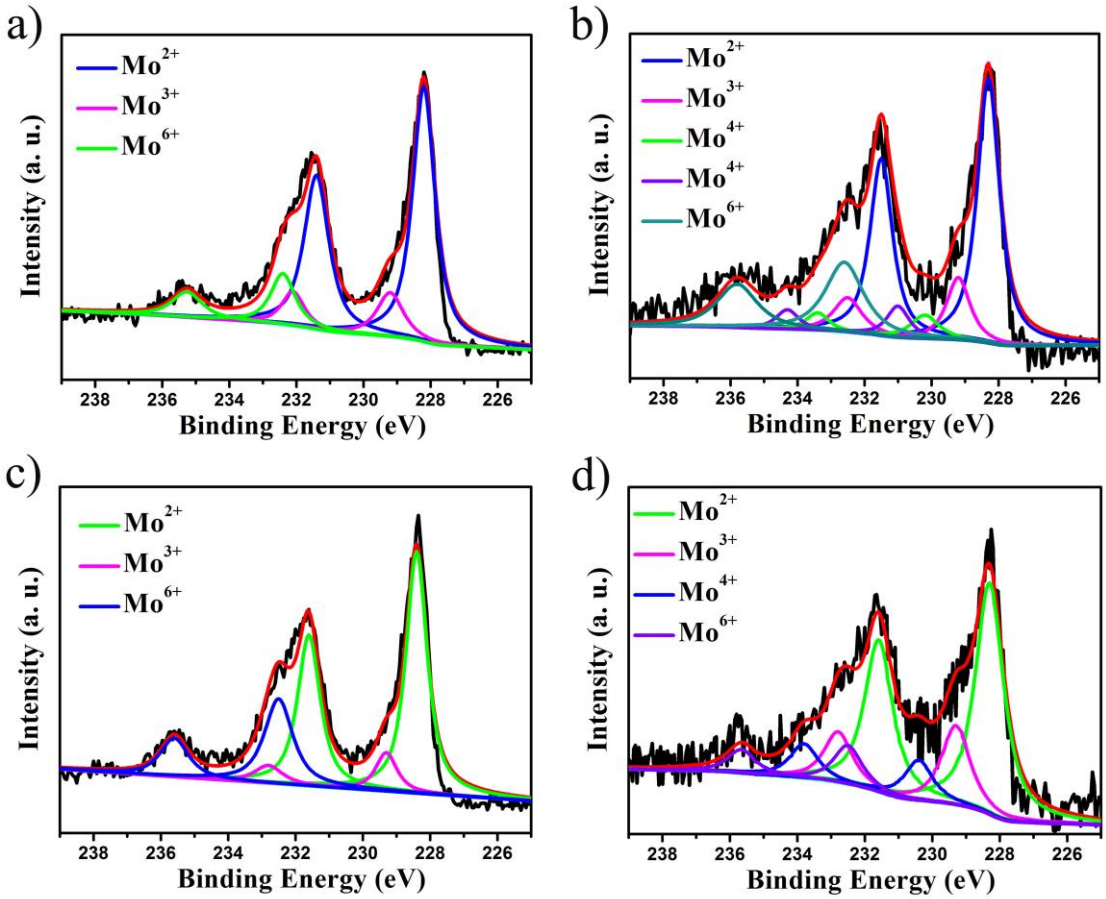

Fig. S38 (a) – (d) The high resolution Mo 3d XPS of **Co/Mo_3Co_3C/Mo_2C@C**, **Co_2P/Mo_3Co_3C/Mo_2C@C**, **Ni/Mo_2C@C** and **Ni/Ni_2P/Mo_2C@C**.

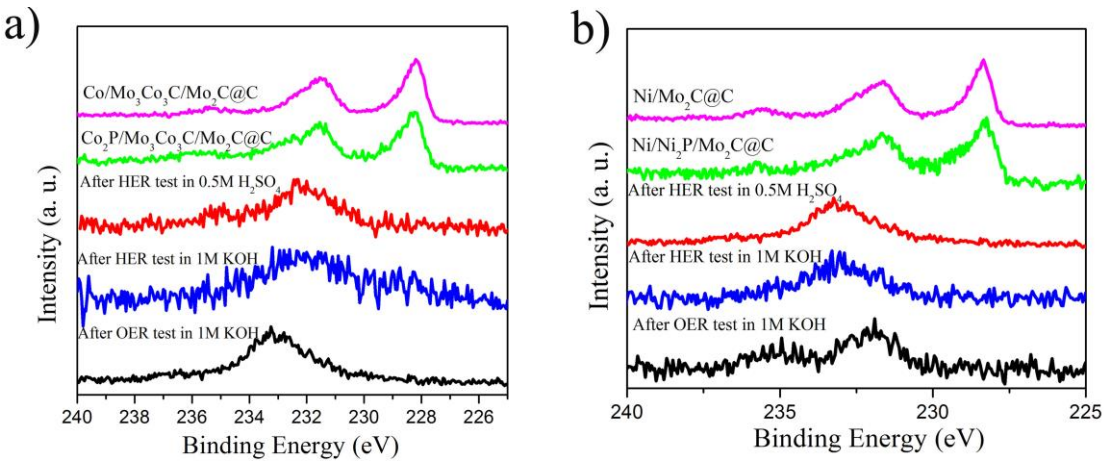

Fig. S39 (a) – (b) The high resolution Mo 3d XPS of **Co_2P/Mo_3Co_3C/Mo_2C@C** and **Ni/Ni_2P/Mo_2C@C** before and after HER and OER tests.

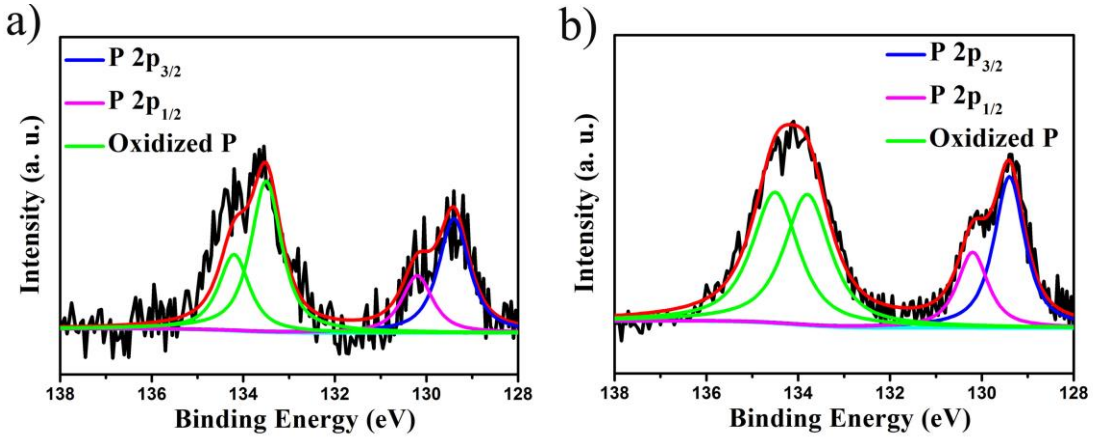

Fig. S40 (a) – (b) The high resolution P 2p XPS of **$Co_2P/Mo_3Co_3C/Mo_2C$@C** and **$Ni/Ni_2P/Mo_2C$@C**.

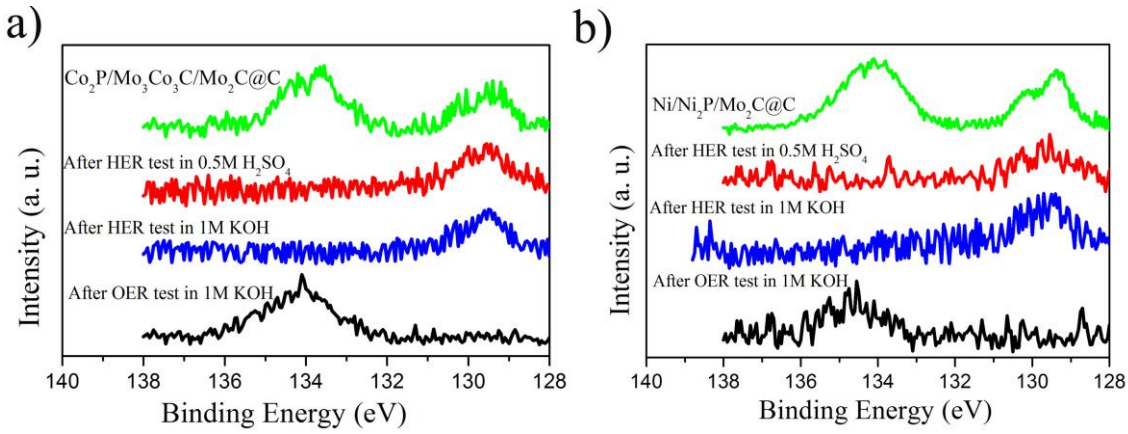

Fig. S41 (a) – (b) The high resolution P 2p XPS of **$Co_2P/Mo_3Co_3C/Mo_2C$@C** and **$Ni/Ni_2P/Mo_2C$@C** before and after HER and OER tests.

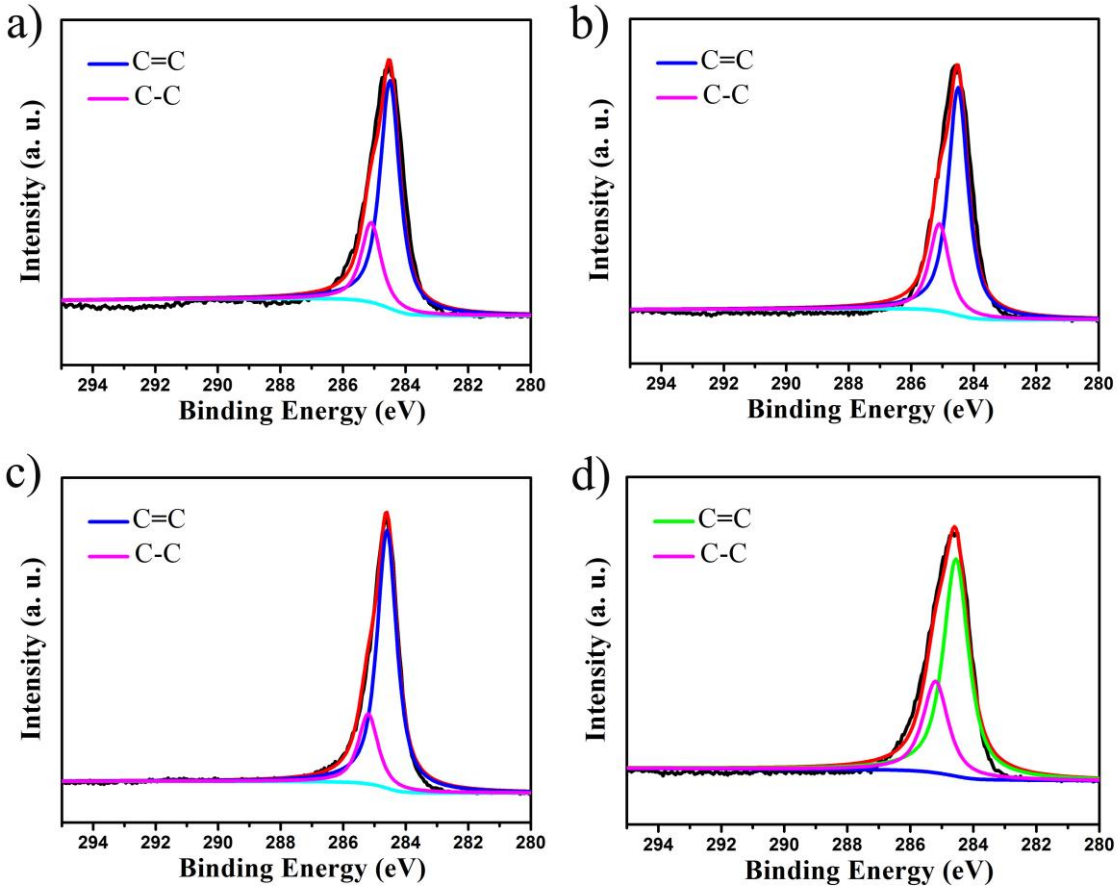

Fig. S42 (a)-(d) The high resolution C 1s XPS of **Co/Mo_3Co_3C/Mo_2C@C**, **Co_2P/Mo_3Co_3C/Mo_2C@C**, **Ni/Mo_2C@C** and **Ni/Ni_2P/Mo_2C@C**. The position of the C 1s line ascribed to C=C is 284.6 eV, downshift by about 0.4 eV compared with GO (285.0 eV), which indicates the charge transfer between the catalysts and grapheme. Moreover, the peak located at about 285.5 is assigned to C-C.

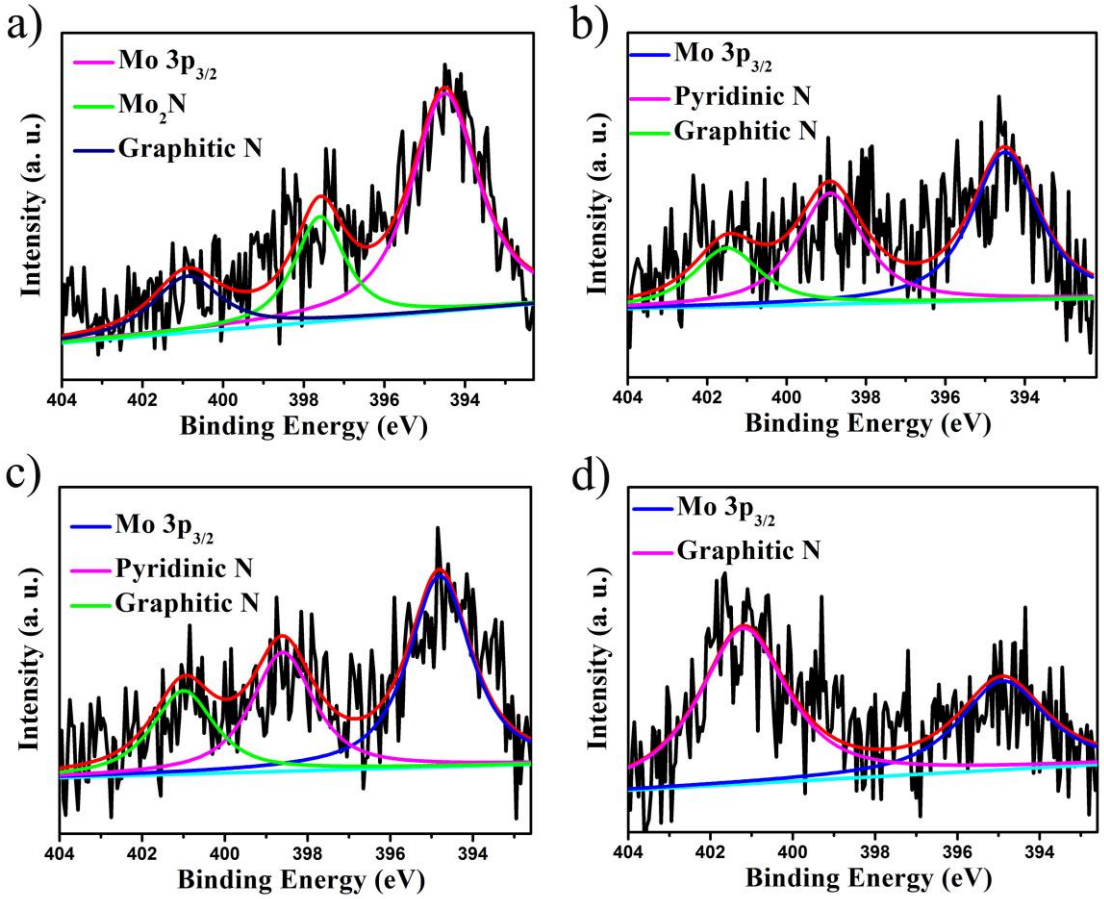

Fig. S43 (a)-(d) The high resolution N 1s XPS of **Co/Mo_3Co_3C/Mo_2C@C**, **Co_2P/Mo_3Co_3C/Mo_2C@C**, **Ni/Mo_2C@C** and **Ni/Ni_2P/Mo_2C@C**.

7. Comparison of HER and OER parameters of different non-Pt catalysts.

Table S4 Comparison for HER activity in acidic solutions for **$Co_2P/Mo_3Co_3C/Mo_2C$@C** and **$Ni/Ni_2P/Mo_2C$@C** with other electrocatalysts.

Catalysts	Loading mass (mg cm^{-2})	Current density (j, mA cm^{-2})	η at correspongding j (mV)	Tafel slope (mV dec^{-1})	Ref.
$Co_2P/Mo_3Co_3C/Mo_2C$@C	0.8	10	154	65	This work
$Ni/Ni_2P/Mo_2C$@C	0.3	10	183	66	This work
Mo_2C nanotubes	0.75	10	172	63	Angew. Chem. Int. Ed. 2015, 54, 15395
MoC_x nano-octaherons	0.8	10	142	53	Nat. Commun. 2015, 6, 6512
Ni_2P nanoparticles	1.0	20	130	46	J. Am. Chem. Soc. 2013, 135, 9267
CoP-CNT	0.285	10	122	54	Angew. Chem. Int. Ed. 2014, 53, 6710
$NiMoN_x$/C	--	2	170	35.9	Angew. Chem. Int. Ed. 2012, 51, 6131
$Co_{0.6}Mo_{1.4}N_2$	--	10	200	--	J. Am. Chem. Soc. 2013, 135, 19186
CoNi@NC	1.6	10	142	104	Angew. Chem. Int. Ed. 2015, 54, 2100
$Ni_{12}P_5$/Ti	1	10	137	63	ACS Nano, 2014, 8, 8121
CoP/rGO-0.36	0.29	10	250	104.8	J. Mater. Chem. A, 2015, 3, 5337
CoP/CNT	0.285	10	122	54	Angew. Chem. Int. Ed. 2014, 126, 6828

Table S5 Comparison for HER activity in basic solutions for **$Co_2P/Mo_3Co_3C/Mo_2C@C$** and **$Ni/Ni_2P/Mo_2C@C$** with other electrocatalysts.

Catalysts	Loading mass (mg cm^{-2})	Current density (j, mA cm^{-2})	η at correspongding j (mV)	Tafel slope (mV $decade^{-1}$)	Ref.
$Co_2P/Mo_3Co_3C/Mo_2C@C$	0.8	10	182	65	This work
$Ni/Ni_2P/Mo_2C@C$	0.3	10	223	68	This work
CoP/CC	0.92	10	210	129	J. Am. Chem. Soc. 2014, 136, 7587
Ni-Decorated Mo_2C	0.12	10	123	84	Chem. Mater. 2016, 28, 6313
Co_2P nanorods	1	20	170	--	Nano Energy 2014, 9, 373
MoC_x nano-octaherons	0.8	10	151	59	Nat. Commun. 2015, 6, 6512
Co-P/NC	0.283	10	191	51	Chem. Mater. 2015, 27, 7636
Ni_2P	1.0	20	205	--	J. Am. Chem. Soc. 2013, 135, 9267.
MoB	2.3	10	225	--	Angew. Chem. Int. Ed. 2012, 51, 12703

Table S6 Comparison for OER activity in basic solutions for **$Co_2P/Mo_3Co_3C/Mo_2C$@C** and **$Ni/Ni_2P/Mo_2C$@C** with other electrocatalysts.

Catalysts	Loading mass (mg cm^{-2})	Current density (j, mA cm^{-2})	η at correspongding j (mV)	Tafel slope (mV $decade^{-1}$)	Ref.
$Co_2P/Mo_3Co_3C/Mo_2C$@C	0.8	10	362	82	This work
$Ni/Ni_2P/Mo_2C$@C	0.3	10	368	75	This work
Ni_2P	0.14	10	290	59	Energy Environ. Sci. 2015, 8, 2347
Co-P films	2.52(Co)	10	345	47	Angew. Chem. Int. Ed. 2015, 54, 6251
$NiCo(OH)_x$	0.2	10	410	109	Adv. Energy Mater. 2015, 5, 1401880
NiCo LDH	0.17	10	367	62	Nano Lett. 2015, 15, 1421
Bulk NiCo LDH	0.07	10	385	65	Nat. Commun. 2014, 5, 4477
$NiCoO_x$	--	10	380	--	J. Am. Chem. Soc. 2013, 135, 16977
CoO/NG		10	340	71	Energy Environ. Sci. 2014, 7, 609
CoOx film	--	10	403	42	J. Am. Chem. Soc. 2012, 134, 17253
Ni/Mo_2C-PC	0.50	10	368	--	Chem. Sci. 2017, 8, 968

Table S7 Comparison for the bifunctional water-splitting activity in basic solutions for **$Co_2P/Mo_3Co_3C/Mo_2C@C$** and **$Ni/Ni_2P/Mo_2C@C$** with other electrocatalysts.

Catalysts	Loading mass (mg cm^{-2})	Current density (*j*, mA cm^{-2})	η at correspongding *j* (V)	Ref.
$Co_2P/Mo_3Co_3C/Mo_2C@C/CC$	0.8	10	1.74	This work
$Ni/Ni_2P/Mo_2C@C$	0.3	10	1.78	This work
NiFe LDH/NF	--	10	1.70	Science 2014, 345, 1593
$Ni(OH)_2$/NF	--	10	1.82	Science 2014, 345, 1593
Ni_3S_2/NF	1.6	13	1.76	J. Am. Chem. Soc. 2015, 137, 14023
CoP_x/NC	1.0	10	~ 1.71	Chem. Mater. 2015, 27, 7636
Ni_5P_4/NF	3.5	10	1.69	Angew. Chem. Int. Ed. 2015, 54, 12361
Pristine NiFeOx/CFP	1.6	10	~1.88	Nat. Commun. 2015, 6, 7261
CoP/rGO-400	0.28	10	1.71	Chem. Sci., 2016, 7, 1690
Ni/Mo_2C-PC/NF	0.50	10	1.66	Chem. Sci., 2017, 8, 968